Geophysical Journal International

Geophys. J. Int. (2013) **193,** 78–97 doi: 10.1093/gji/ggs126

The Davis Strait crust—a transform margin between two oceanic basins

Sonja K. Suckro,[1] Karsten Gohl,[1] Thomas Funck,[2] Ingo Heyde,[3] Bernd Schreckenberger,[3] Joanna Gerlings[2,4] and Volkmar Damm[3]

[1]*Alfred Wegener Institute for Polar and Marine Research (AWI), Am Alten Hafen* 26, 27568 *Bremerhaven, Germany. E-mail: Sonja.Suckro@awi.de*
[2]*Geological Survey of Denmark and Greenland (GEUS), Øster Voldgade* 10, DK-1350 *Copenhagen K, Denmark*
[3]*Federal Institute for Geosciences and Natural Resources (BGR), Stilleweg* 2, 30655 *Hanover, Germany*
[4]*Dalhousie University, Department of Earth Sciences,* 1459 *Oxford Street, Halifax, N.S.,* B3H 4R2, *Canada*

Accepted 2012 December 21. Received 2012 December 11; in original form 2012 August 8

SUMMARY

The Davis Strait is located between Canada and Greenland and connects the Labrador Sea and the Baffin Bay basins. Both basins formed in Cretaceous to Eocene time and were connected by a transform fault system in the Davis Strait. Whether the crust in the central Davis Strait is oceanic or continental has been disputed. This information is needed to understand the evolution of this transform margin during the separation of the North American plate and Greenland. We here present a 315-km-long east–west-oriented profile that crosses the Davis Strait and two major transform fault systems—the Ungava Fault Complex and the Hudson Fracture Zone. By forward modelling of data from 12 ocean bottom seismographs, we develop a *P*-wave velocity model. We compare this model with a density model from ship-borne gravity data. Seismic reflection and magnetic anomaly data support and complement the interpretation. Most of the crust is covered by basalt flows that indicate extensive volcanism in the Davis Strait. While the upper crust is uniform, the middle and lower crust are characterized by higher *P*-wave velocities and densities at the location of the Ungava Fault Complex. Here, *P*-wave velocities of the middle crust are 6.6 km s^{-1} and of the lower crust are 7.1 km s^{-1} compared to 6.3 and 6.8 km s^{-1} outside this area; densities are 2850 and 3050 kg m^{-3} compared to 2800 and 2900 kg m^{-3}. We here interpret a 45-km-long section as stretched and intruded crust or as new igneous crust that correlates with oceanic crust in the southern Davis Strait. A high-velocity lower crust (6.9–7.3 km s^{-1}) indicates a high content of mafic material. This mantle-derived material gradually intruded the lower crust of the adjacent continental crust and can be related to the Iceland mantle plume. With plate kinematic modelling, we can demonstrate the importance of two transform fault systems in the Davis Strait: the Ungava Fault Complex with transpression and the Hudson Fracture Zone with pure strike-slip motion. We show that with recent poles of rotation, most of the relative motion between the North American plate and Greenland took place along the Hudson Fracture Zone.

Key words: Plate motions; Transform faults; Continental margins: divergent; Crustal structure; Arctic region.

1 INTRODUCTION

The Davis Strait is located between Canada and Greenland and connects the Baffin Bay in the north with the Labrador Sea in the south (Fig. 1). The strait is a bathymetric high with water depths <700 m, while the water depth in the Baffin Bay and the Labrador Sea exceeds 2000 m. Prominent tectonic features of the Davis Strait are the Ungava Fault Complex and the Davis Strait High. A line of positive southwest–northeastward striking free-air gravity anomalies marks the location of the Ungava Fault Complex, a major transform fault (Funck *et al.* 2007; Gregersen & Skaarup 2007; Gerlings *et al.* 2009). In the centre of the strait, the Davis Strait High is characterized by outcropping basement between 66 and 67°N (Dalhoff *et al.* 2006).

The Davis Strait area has experienced Paleogene volcanism. Outcrops of volcanic sequences are located on Disko Island and the adjacent Nuussuaq Peninsula (Storey *et al.* 1998; Pedersen *et al.* 2006). On the Canadian margin, volcanics are mapped at Cape Dyer (Clarke & Upton 1971) and offshore in seismic reflection data (Skaarup *et al.* 2006). Volcanics are drilled offshore at several wells as indicated in Fig. 1(a).

The Davis Strait crust has long been a subject of debate. Sonobuoy readings reveal a 22-km-thick crust, which is interpreted as a thick pile of oceanic crust by Keen & Barrett (1972). Chalmers &

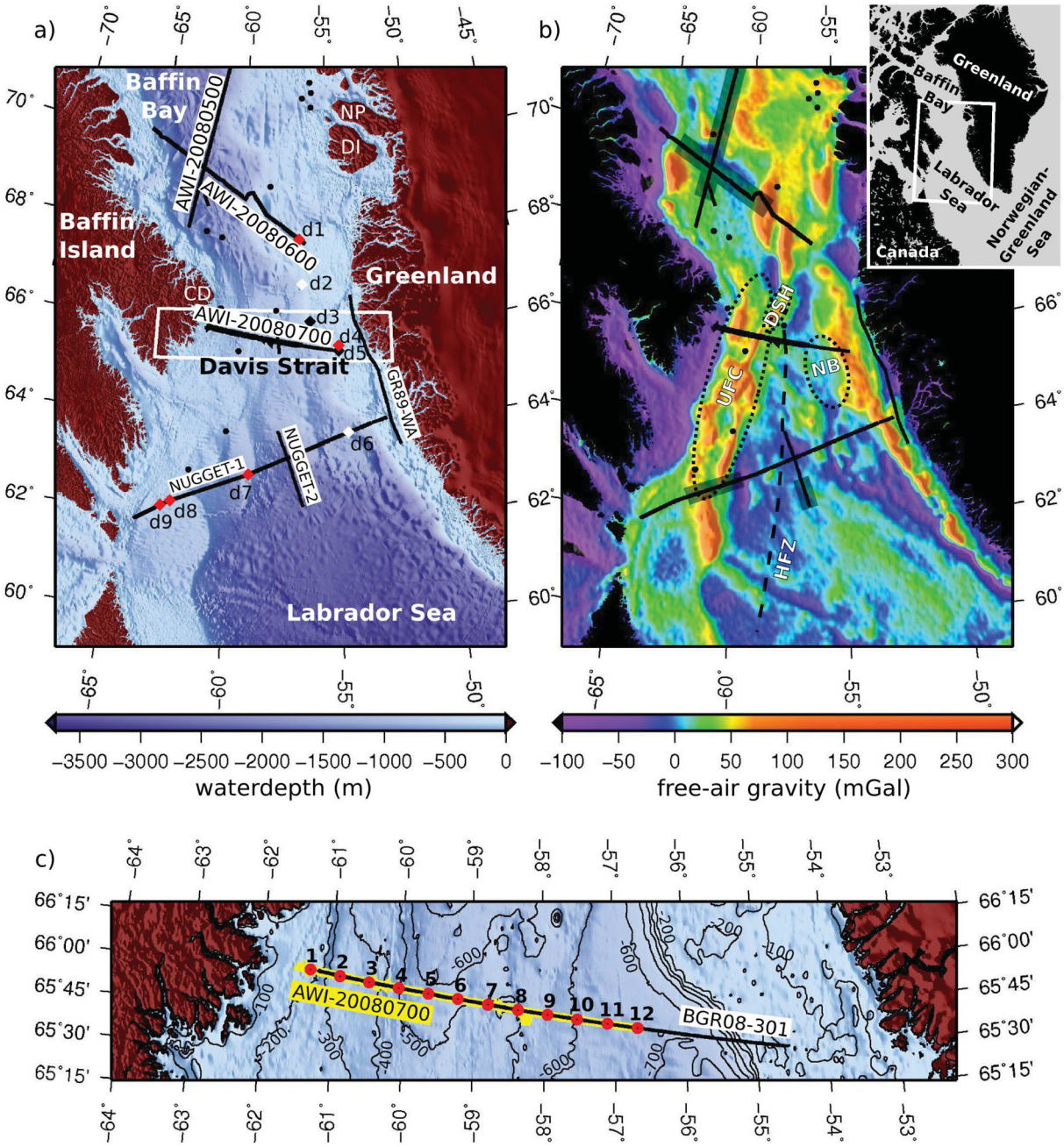

Figure 1. (a) Bathymetric map of the Davis Strait area (GEBCO_08 Grid, Version 20090202, http://www.gebco.net) with place names and locations of wide-angle seismic data. Abbreviations are: (NP) Nuussuaq Peninsula, (DI) Disko Island, (CD) Cape Dyer. Line AWI-2008500, -600, -700 were acquired during the MSM09/3 cruise of RV Merian in 2008 (Gohl *et al.* (2009); Funck *et al.* (2012); Suckro *et al.* (2012)); black dots and short black lines are locations of sonobuoys and profiles of expandable sonobuoys from Keen & Barrett (1972); NUGGET-1 (Funck *et al.* 2007), NUGGET-2 (Gerlings *et al.* 2009), and GR89-WA (Gohl & Smithson 1993) are seismic refraction lines; diamonds mark well locations: (d1) Hellefisk-1, (d2) Ikermiut, (d3) Kangamiut-1, (d4) Nukik-2, (d5) Nukik-1, (d6) Qulleq-1, (d7) Gjoa G-37, (d8) Ralegh N-18, (d9) Hekja O-71; red diamonds: volcanics are drilled; black diamonds: Precambrian rocks are drilled; white diamonds: neither is drilled; all well information are from the Natural Resources Canada, originator: Phil Moir. (b) Free-air gravity anomalies derived from satellite altimetry of the offshore area (Sandwell & Smith 2009), version 18.1; grey shaded areas mark the extend of oceanic crust on seismic refraction lines (Funck *et al.* 2007; Gerlings *et al.* 2009; Funck *et al.* 2012; Suckro *et al.* 2012); positive gravity anomalies that mark the Ungava Fault Complex (UFC) are circled, as is the Davis Strait High (DSH) and the Nuuk Basin (NB); location of the Hudson Fracture Zone (HFZ) after Chalmers & Pulvertaft (2001). (c) Closeup of the coinciding seismic refraction line AWI-20080700 with OBS locations marked by red dots and line BGR08-301 with seismic reflection, gravity and magnetic anomaly data.

Pulvertaft (2001) interpret the crust as continental, while Srivastava *et al.* (1982) argue that the Davis Strait High is a continental block and the adjacent basins are underlain by oceanic crust. A seismic refraction line in southern Davis Strait showed that continental crust is separated by a 140-km-wide zone of oceanic crust (NUGGET-1, Funck *et al.* 2007, Fig. 1b).

To determine the nature of the crust in the central Davis Strait, a 226-km-long seismic refraction profile was recorded during the

cruise MSM09/3 of RV Maria S. Merian in 2008 (Gohl *et al.* 2009). Additionally, multi-channel seismic reflection (MCS), ship-borne gravity and magnetic field data were collected on the same line with an additional 90 km extend to the east. We here present the results of *P*-wave velocity and gravity forward modelling together with magnetic field and MCS data. The results are used in a plate kinematic model to determine the role of the Ungava Fault Complex in the evolution of the Davis Strait.

2 TECTONIC BACKGROUND OF THE OPENING OF THE LABRADOR SEA AND THE BAFFIN BAY

The tectonic evolution of the Davis Strait is linked to the evolution of the Baffin Bay and the Labrador Sea. These have formed in the Cretaceous to Eocene during the separation of Greenland from the North American craton (e.g. Chalmers & Pulvertaft 2001; Tessensohn & Piepjohn 2000). The time of initial rifting of North America and Greenland is dated to earliest Cretaceous by Larsen *et al.* (1999) from dyke intrusions in southern West Greenland. On the Nuussuaq Peninsula, tectonic instability with three phases of uplift occurred in the Maastrichtian (Chalmers *et al.* 1999). The age of the oldest oceanic crust in the Labrador Sea is disputed. Roest & Srivastava (1989) date it to magnetic chron 33 (80 Ma after Gradstein *et al.* 2004, which is used throughout this paper for dating), while Chalmers & Laursen (1995) use chron 27N (62 Ma). Recent seismic refraction and gravity data have now confirmed Paleocene and Eocene oceanic crust in southern Baffin Bay (Funck *et al.* 2012; Suckro *et al.* 2012).

A first volcanic pulse at 60.7–59.4 Ma is identified from volcanics on Disko Island by Storey *et al.* (1998) and correlated with the arrival of the Greenland–Iceland mantle plume in the Davis Strait area. (Funck *et al.* 2007) attribute a thick high-velocity lower crust in their *P*-wave velocity model of the NUGGET-1 line to the southward flow of plume material.

During magnetic chron 24R (55 Ma), the relative motion of Greenland to the North American craton changed from east to northeast, as indicated by magnetic spreading anomalies in the Labrador Sea (Roest & Srivastava 1989; Oakey 2005). This caused new fractures and the breaking of Paleocene oceanic crust in the southern Baffin Bay and the evolution of new spreading centres in the Eoecene (Chalmers & Pulvertaft 2001; Oakey 2005; Suckro *et al.* 2012). The opening of the Norwegian–Greenland Sea is dated to chron 24 (Talwani & Eldholm 1977; Olesen *et al.* 2007), therefore, Greenland moved as an independent plate from this time until the end of relative motion between Greenland and the North American craton (Tessensohn & Piepjohn 2000). According to Storey *et al.* (1998), the reorientation of spreading caused a second volcanic pulse at 54.8–53.6 Ma in the Disko Island area.

Spreading ceased in the Labrador Sea at chron 13 (33 Ma) according to Srivastava (1978), while separation of Greenland and Eurasia and the opening of the Northeast Atlantic are still ongoing. Since then sedimentation and subsidence are the dominant geologic processes in the Baffin Bay and the Labrador Sea (Chalmers & Pulvertaft 2001).

The Ungava Fault Complex consists of several northeast–southwest striking faults that are oriented along positive gravity anomalies in the Davis Strait (Fig. 1b, Sørensen 2006). The Ungava Fault Complex marks the northwestern border of oceanic crust in the Labrador Sea (Chalmers & Pulvertaft 2001). It is interpreted as a transform system, linking seafloor spreading in the Labrador Sea with spreading in the Baffin Bay (Rice & Shade 1982; Chalmers & Pulvertaft 2001). Skaarup *et al.* (2006) interpret the Ungava Fault Complex in the Davis Strait as the continent–ocean boundary of the Greenland plate. East of the Ungava Fault Complex runs the north–south striking Hudson Fracture Zone, which meets the Ungava Fault Complex in the Davis Strait (Chalmers & Pulvertaft 2001). The Hudson Fracture Zone was first identified from magnetic anomaly data by Srivastava (1978).

3 DATA ACQUISITION

Seismic and potential field data of this study were acquired during the research cruise MSM09/3 of RV Maria S. Merian in 2008 (Gohl *et al.* 2009). The profiles presented here were set up to determine the crustal thickness and structure across the Davis Strait and the Ungava Fault Complex (Fig. 1).

We collected seismic refraction data along the 226-km-long profile AWI-20080700 with 12 ocean bottom seismometers (OBS) (Fig. 1c). Technical details are listed in Table 1. On line BGR08-301, we recorded MCS and potential field data. BGR08-301 coincides with line AWI-20080700 and extends 90 km further eastwards (Fig. 1c). Setup parameters of the MCS measurement are summarized in Table 2.

Gravity data were recorded with a KSS31M sea gravimeter (Bodensee Gravitymeter Geosystem GmbH) at 1 Hz sampling rate. To reference the ship-borne gravity data, we carried out connection measurements on land with a LaCoste&Romberg gravity metre at the beginning and end of the cruise (Gohl *et al.* 2009). Magnetic field data were recorded with an Overhauser SeaSPY marine magnetometer system towed approximately 600 m behind the vessel.

4 SEISMIC DATA

4.1 Seismic reflection data

The MCS data are common depth point (CDP) sorted to 6.25 m and processed with ProMAX^{TM} with the processing steps listed in Table 3. We were able to remove the first seafloor multiple by a surface-related multiple estimation procedure. The trade-off of this

Table 1. Setup parameters of the seismic refraction survey.

OBS type	3-component Mark seismometers, 4.5 Hz natural frequency, 1 hydrophone
OBS spacing	nominally 18 km
Seismic source	array of 16 G.Guns^{TM} and 2 Bolt^{TM} guns
Volume G.Gun^{TM} array	50.8 L, 3100 in^3
Operation pressure	145 bar
Volume 2 Bolt^{TM} guns	64 L, 3906 in^3
Operation pressure	120 bar
Total source volume	114.8 L, 7006 in^3
Shot interval	60 s

Table 2. Setup parameters of the seismic reflection survey.

Streamer length	3450 m
Number of channels	276
Sampling rate	2 ms
Recording length	14 s
Seismic source	array of 16 G.Guns^{TM}
Operation pressure	100–135 bar
Total source volume	50.8 L, 3100 in^3
Shot interval	18 s

Table 3. Processing steps applied to the MCS data of line BGR08-301 in ProMAX™.

Resampling: 4 ms
Apply geometry: common mid point binning of 6.25 m
Bandpass filter: (4 -) 8–80 (- 160) Hz
Velocity analysis
Surface related multiple estimation
Velocity analysis
Predictive deconvolution
Normal move out correction
Stack
Poststack Kirchhoff migration

procedure is that primary signals are also partly absorbed (white band between 1 and 2 s from a model distance of 90–290 km, Fig. 2). Multiples that are not suppressed by this procedure are multiples of the basement at distances of 0–70 and 95–135 km. At these locations, the acoustic basement is close to the seafloor (less than 0.1 s two-way traveltime) and the remaining basement multiples can easily be confused with seafloor multiples. But their shape varies from the seafloor morphology, especially at 40 and 115 km model distance (Fig. 2).

We interpret the acoustic basement from the seismic reflection data in order to use it in the *P*-wave velocity and the density models. From distances of 70–95 and 165–325 km, the basement is the lowest continuous reflector and marks the base of stratified sedimentary sequences. From a distance of 135–165 km, we use the top of a series of high-amplitude reflectors below a more transparent sediment succession. The base of these high-amplitude reflectors cannot be defined from the seismic reflection data, but in combination with the *P*-wave velocity and density model, an interpretation is discussed later. The deformation of sediments in this section will be discussed later and is therefore highlighted in closeup B of Fig. 2. As mentioned before, distances of 0–70 and 95–135 km are only covered by very little sediment. Here, the basement morphology is best determined from the basement multiples. Dipping reflector sequences from a distance of 55–67 km are also better visible in the multiple (closeup A in Fig. 2).

Table 4. Statistical values of the *P*-wave velocity model calculated by rayinvr and dmplstsqr (Zelt & Smith 1992). *n* is the number of observations; pick uncertainties are averaged for all observations; RMS is the misfit between calculated and observed traveltime; the normalized χ^2 is a measure of how well-calculated traveltimes are within the range of the pick uncertainty.

Layer	*n*	Pick uncertainty (ms)	RMS (ms)	Normalized χ^2
$P_{sa} - P_{sd}$	424	67	47	0.527
$P_{sa}P - P_{sd}P$	211	89	70	0.915
P_{se}	644	82	48	0.401
$P_{se}P$	288	90	99	1.040
P_{bas}	84	92	46	0.278
$P_{LVZ}P$	113	70	50	0.296
P_{c1}	707	100	68	0.692
$P_{c1}P$	188	115	100	1.006
P_{c2}	2647	123	170	2.261
$P_{c2}P$	429	166	153	0.764
P_{c3}	1217	189	279	2.064
P_mP	1286	158	351	4.682
P_n	221	200	109	0.300
Total	8459	131	177	1.965

4.2 *P*-wave velocity model

We relocalized the OBS positions with the arrival of the direct wave. All refracted and reflected signals were picked with the software zp (by B. Zelt, www.soest.hawaii.edu/users/bzelt/index.html), using a bandpass filter of 4–15 Hz applied for the near offset signals (30 km distance from the station) and 4–10 Hz for greater offsets. Picking errors were assigned manually to each phase, taking into account the signal to noise ratio. In Table 4, the assigned pick uncertainties are summarized for each phase. Refracted phases are named as P_{layer} and reflected phases $P_{\text{layer}}P$, except for the reflection at the Moho, P_mP, and the refraction in the upper mantle, P_n.

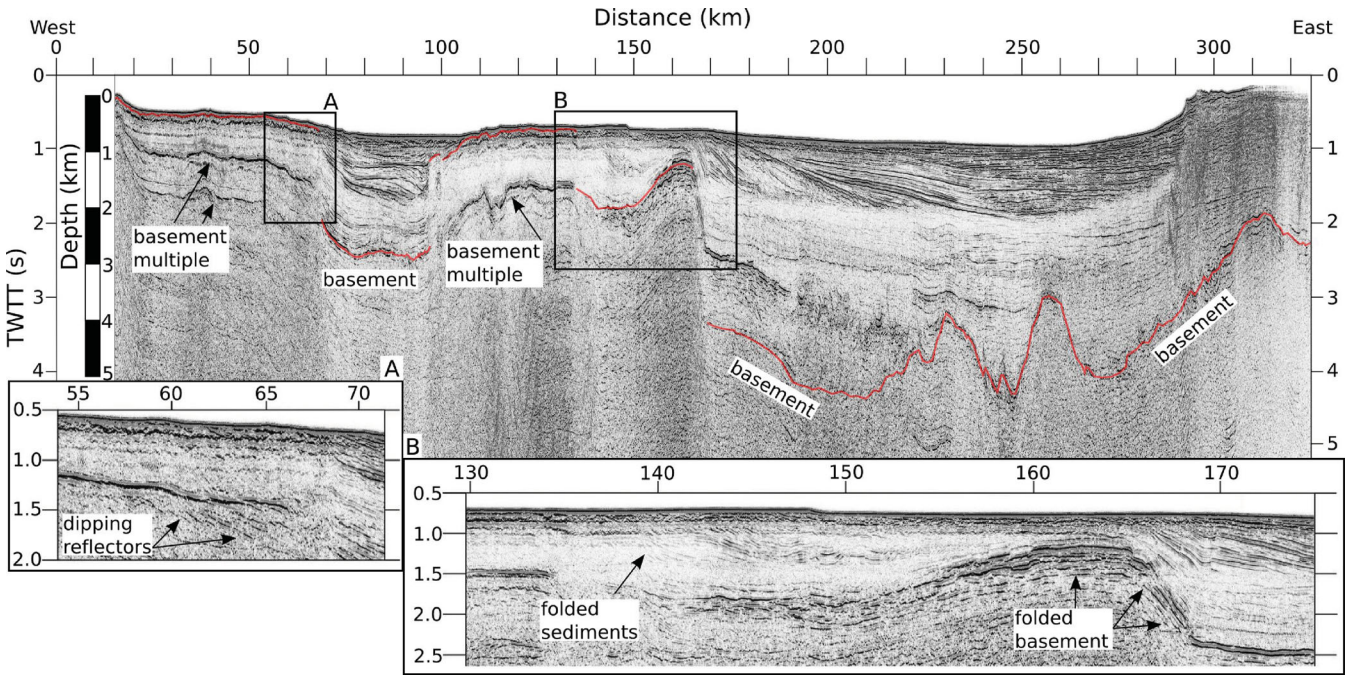

Figure 2. Final processing of MCS data along line BGR08-301; basement is marked in red; depth scale is approximated by average *P*-wave velocities of sediments along the profile. Closeup A shows dipping reflectors in the basement multiple. Closeup B shows folded sediments.

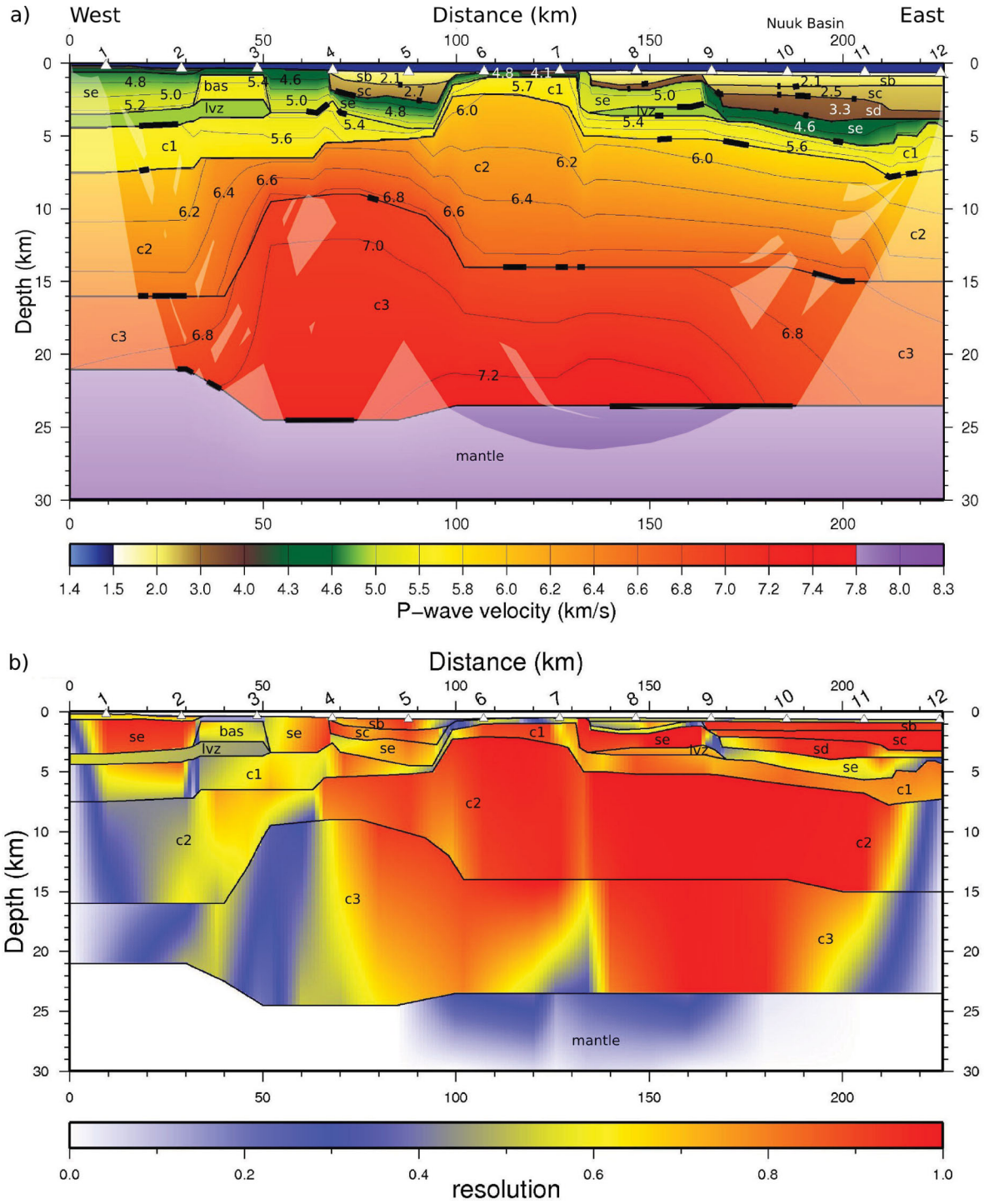

Figure 3. (a) *P*-wave velocity model with layer names. Interpretation of the layers are: sb, sc, sd are sediments; se are basalts intercalated with sediments; bas is a basalt unit; lvz abbreviates low velocity zone and represents buried sediments; c1 is the upper crust, c2 the middle crust and c3 the lower crust. White triangles indicate OBS locations; rotated numbers are OBS numbers; numbers on contour lines are *P*-wave velocities in km s^{-1}; thick lines mark layer boundaries that are constrained by reflected phases; white shaded areas are not passed by rays. (b) Gridded diagonal values of the resolution matrix of the *P*-wave velocity model. Layers are annotated; white triangles indicate OBS locations; rotated numbers are OBS numbers.

By forward modelling with the software rayinvr (Zelt & Smith 1992), we obtained the *P*-wave velocity model in Fig. 3. Ray coverage of the single layers is displayed in Fig. 4; modelling of all stations is given in the Appendix in Figs A1 and A2; examples of modelling for OBS 2, 8 and 11 are displayed in Figs 5–7. The modelled layers are described in the following paragraphs. The accuracy of the model depends on the data coverage and quality; typical uncertainties of the *P*-wave velocity are ± 0.1 km s^{-1}.

Water: For the seawater, we used an average velocity of 1.47 km s^{-1}, which was calculated from a conductivity temperature density (CTD) measurement during the cruise (Gohl *et al.* 2009). We took the depth of the seafloor from bathymetry data of the on-board multi-beam echo-sounder.

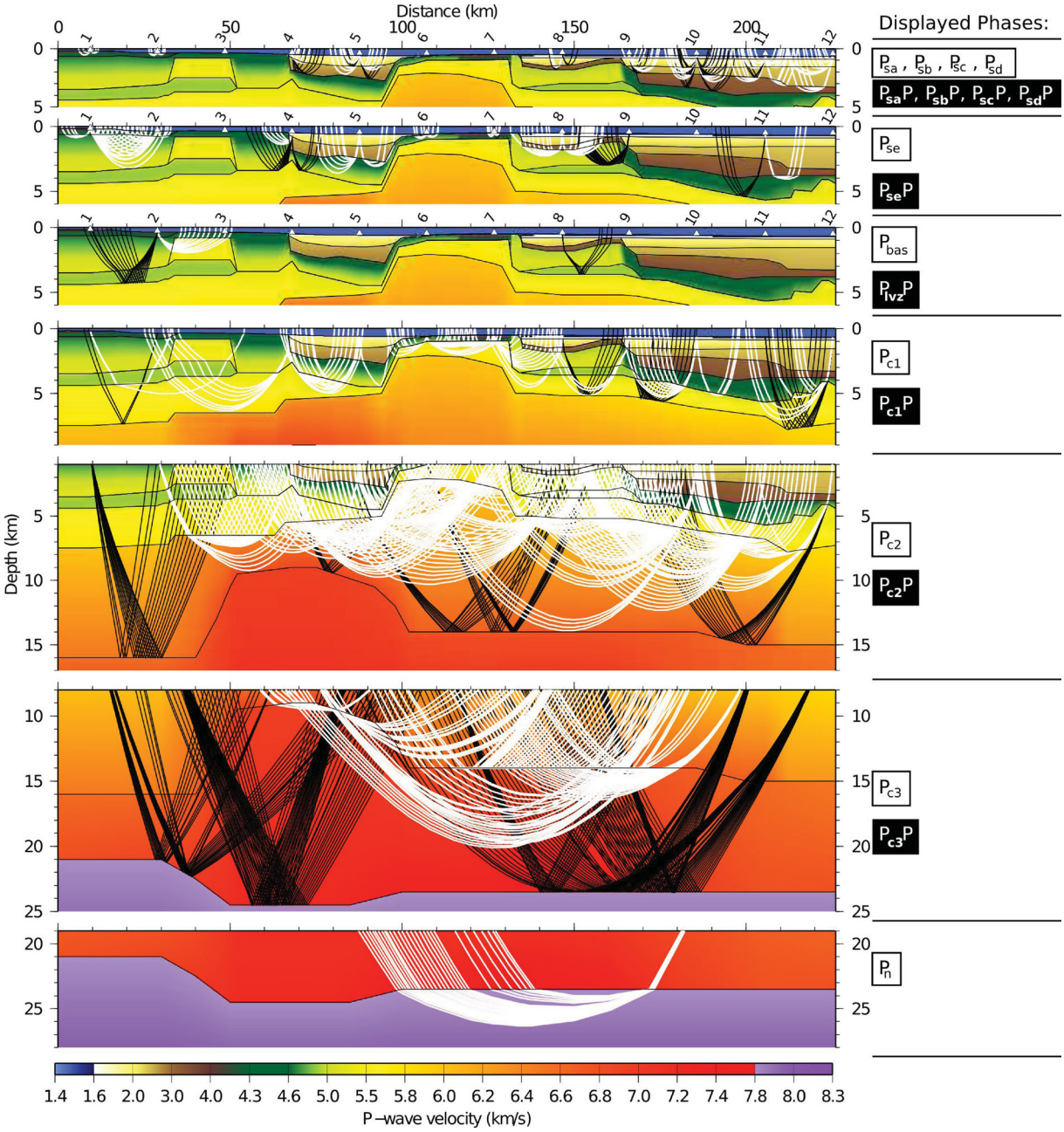

Figure 4. Ray coverage of the different layers in the *P*-wave velocity model (Fig. 3). Refracted phases are displayed in white, reflected in black.

sa, sb, sc, sd: Sediment layers with *P*-wave velocities ranging from 1.5 to 3.5 km s^{-1} are determined from the OBS data (Fig. 3). The complex structure of the basement is incorporated from the high-resolution MCS data (Fig. 2).

From a model distance of 68–100 km, a sediment basin with *P*-wave velocities from 1.8 to 2.9 km s^{-1} is modelled from phases of OBS 4 and 5 (Figs 3 and 4). The sediment infill of the basin at a model distance of 135–165 km consists of two units. A 1-km-thick unit with *P*-wave velocities of 1.5–2.4 km s^{-1} overlies a 0.5-km-thick unit with an average *P*-wave velocity of 3.3 km s^{-1} (Fig. 3). The low velocity of the upper unit is extrapolated from the sediment package of the eastern basin. The lower sediment unit is confirmed by P_{sd} phases of OBS 8 (Fig. 4). The sediments east of a model distance of 165 km, in the Nuuk Basin, are of similar character. A 2-km-thick sediment sequence with *P*-wave velocities of 1.5–2.6 km s^{-1} overlies a 1-km-thick unit with an average *P*-wave velocity of 3.3 km s^{-1} (Fig. 3). P_{sb}, P_{sc} and P_{sd} phases from OBS 9 to 12 confirm these sequences (Fig. 4).

se: We later interpret this layer, with *P*-wave velocities between 4.1 and 5.1 km s^{-1}, partly as basalts and therefore name it here separately from the other sediment layers.

At a model distance of 0–68 km, this layer is modelled with *P*-wave velocities of 4.4–5.5 km s^{-1} according to P_{se} phases of OBS 1, 2 and 4 (Figs 3, 4 and A1). From a model, distance of 35–50 km lies a body of higher velocities (5.4 km s^{-1}). From a model distance of 68–95 km, the layer **se** is modelled with 2 km thickness and is confirmed by P_{se} phases of OBS 5 (Figs 3 and A1). From a model distance of 95–135 km, the layer **se** is only 0.5 km thick and modelled with a *P*-wave velocity of 4.8 km s^{-1} west of 117 km (Fig. 3). East of 117 km, a *P*-wave velocity of 4.1 km s^{-1} is

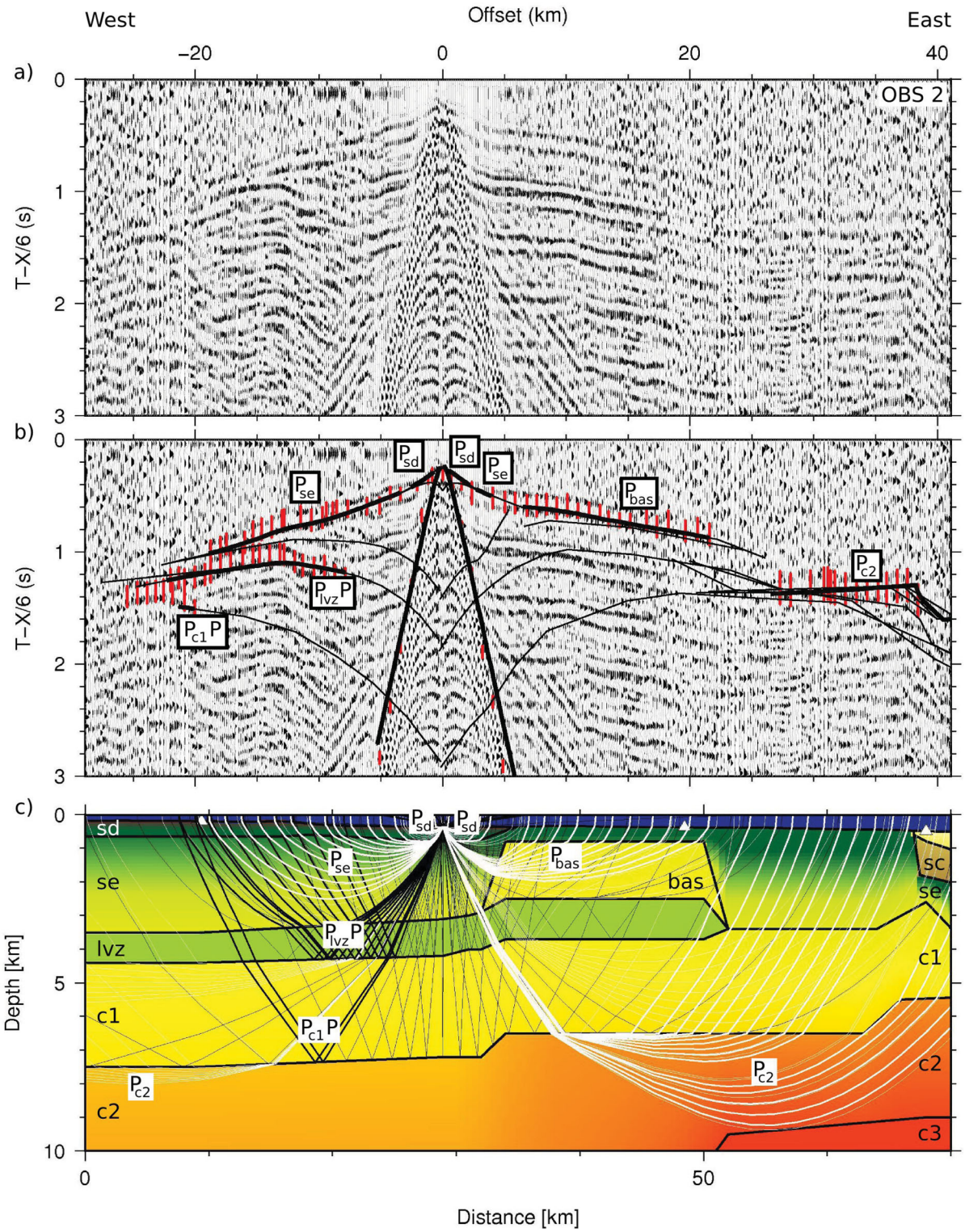

Figure 5. (a) Seismic section of OBS 2, displayed with a reduction velocity of 6 km s^{-1}. (b) The same seismic section with picks in red; the pick length corresponds to the assigned pick uncertainty; calculated traveltimes are displayed in black with thick black lines corresponding to the picks. (c) *P*-wave velocity model with ray paths. Model layers are annotated; black rays indicate reflected phases, white rays refracted phases; thick lines correspond to the picks in the central panel.

modelled. This velocity difference is needed to account for different P_{se} phases from OBS 6 and 7. From a model distance of 135–165 km, the layer **se** is 2 km thick and modelled with 4.9–5.2 km s^{-1}, according to P_{se} phases of OBS 8 (Figs 3 and 4). The thickness is confirmed by OBS 9 (Fig. A2). East of a model distance of 165 km, in the Nuuk Basin, the velocity structure is determined only by a P_{se} phase of OBS 11 (Fig. 7), which indicates a *P*-wave velocity of 4.0 km s^{-1}.

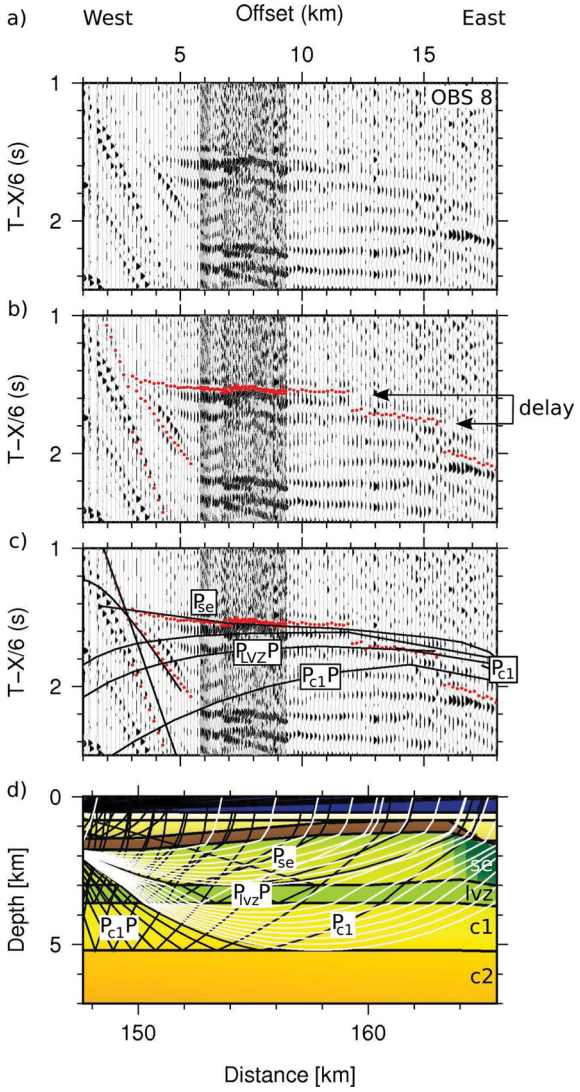

Figure 6. (a) Cutout of the seismic section of OBS 8, displayed with a reduction velocity of 6 km s^{-1}. (b) The same seismic section with picks in red. (c) The same seismic section with picks in red and calculated traveltimes in black. (d) *P*-wave velocity model with ray paths; black rays indicate reflected phases, white rays refracted phases; model layers are annotated.

bas: We modelled a separate body of higher *P*-wave velocities than the surrounding layer **se** from a refracted phase P_{bas} of OBS 2 (Fig. 5). The average *P*-wave velocity is 5.4 km s^{-1} and the thickness is 1.5 km.

lvz: Low-velocity zones (LVZs) are modelled at a model distance of 0–50 km and of 135–170 km. Phases in OBS 1 and 2 indicate a LVZ at a model distance of 0–50 km by fading P_{se} and P_{bas} phases and by a delay of crustal phases (Figs 5 and A1). We chose a velocity of 4.9 km s^{-1} for the LVZ, as this is the average *P*-wave velocity of the surrounding layer **se**. The LVZ from a model distance of 135–170 km was introduced due to delayed phases in OBS 8, as shown in Fig. 6. The delay of 0.14 s is modelled with a 0.6-km-thick layer of *P*-wave velocity of 4.9 km s^{-1}. The *P*-wave velocity of the LVZ has to be smaller than 5.2 km s^{-1}, which is the velocity at the base of the overlying layer. We have chosen 4.9 km s^{-1}, which is the *P*-wave velocity at the top of the overlying layer se. It can therefore be interpreted as part of this layer, which is later interpreted as basalts intercalated with sediments.

c1: *P*-wave velocities of the first crustal layer range from 5.2 km s^{-1} at the top to 5.8 km s^{-1} at the base. The average *P*-wave velocity is 5.5 km s^{-1}, which is well confirmed by P_{c1} phases throughout the model except for the western end of the model (Figs 3 and 4). The thickness varies between 0.5 and 3.5 km along the profile.

From a model distance of 0–68 km, the upper crust (c1) is 2.5–3.0 km thick, while it thins from 3 to 0.5 km eastwards beneath the sediment basin from a model distance of 68–95 km (Fig. 3). From a model distance of 100–210 km, the thickness is more uniform with 1.5–2.0 km. East of a model distance of 210 km, a thickening to 3 km is modelled due to $P_{c1}P$ phases in OBS 11 and 12 (Figs 4 and A2). The top of the upper crust (c1) is modelled from the basement interpretation of the MCS data from a model distance of 135–226 km (Figs 2 and 3).

c2: The second crustal layer is modelled with *P*-wave velocities of 5.9–6.7 km s^{-1}, except for a model distance of 40–95 km where it is characterized by higher *P*-wave velocities of 6.5–6.8 km s^{-1} (Fig. 3). Here, the middle crust (c2) is only 2.5–4 km thick, while it reaches 7.5–12 km thickness in the adjacent model parts. Except for the model boundaries, the velocity structure is well confirmed by P_{c2} phases (Fig. 4). The velocity structure west of a profile distance of 40 km is only confirmed at the top of the layer by OBS 4 (Fig. A1). The velocity at the bottom can thus be chosen in a wide range. An extrapolation of high velocities, such as in the thin lower crust section from 40–95 km, did not lead to the required delay of later crustal phases. We thus adopt a lower velocity structure, similar to the model distances east of 95 km for the western profile termination. Also, from model distances of 210–226 km, we use low *P*-wave velocities of 5.9–6.3 km s^{-1} instead of 5.9–6.7 km s^{-1} to model the delay of later arrivals. Fig. A2 shows that the P_mP phase in OBS 12 has travelled through crust with considerably lower *P*-wave velocities than the P_mP phase in OBS 10 and 11.

c3: The third crustal layer has *P*-wave velocities between 6.5 and 7.4 km s^{-1}. Similar to the middle crust (c2), the lower crust (c3) is characterized by higher *P*-wave velocities in the centre of the model than at the sides (Fig. 3).

At a model distance of 50–160 km, *P*-wave velocity ranges from 6.8 to 7.4 km s^{-1}. At 190–226 km, the average velocity is considerably lower with only 6.7 km s^{-1}. This velocity reduction is necessary to account for the P_mP phase in OBS 12. Fig. A2 shows that even slower velocities are necessary for modelling of OBS 12, but this would then change the fit of P_{c3}, P_mP and P_n phases in OBS 10 and 11 and we thus did not further lower the *P*-wave velocities. Similar to the modelling of the P_mP phase of OBS 12, there is a misfit in the modelling of the P_mP phase of OBS 1. Another possibility of modelling OBS 1 is with a deeper Moho at the eastern termination of the profile. Because this leads to a misfit with the gravity model and with data from OBS 4, we did not chose this option. At both profile terminations, we chose the model that fits best to the data of OBS with good ray coverage and to the gravity model. The lower crust is well resolved from a model distance of 65–190 km by P_{c3} and P_mP phases (Figs 3 and 4). From 0 to 65 km, modelling only depends on P_mP phases (Fig. 4) and *P*-wave velocities are thus not well constrained. The depth of the Moho varies between 21 and 24.5 km and is confirmed by various P_mP phases (Fig. 4).

Mantle: A *P*-wave velocity of 7.8 km s^{-1} is modelled at the top of the mantle from a P_n phase of OBS 11 (Figs 7 and A2).

Table 4 summarizes statistical values as a measure of quality for the model's fit to the picked traveltimes. The root mean square traveltime (RMS) error is calculated by rayinvr from the misfit of calculated and picked traveltime. The normalized χ^2 is a measure

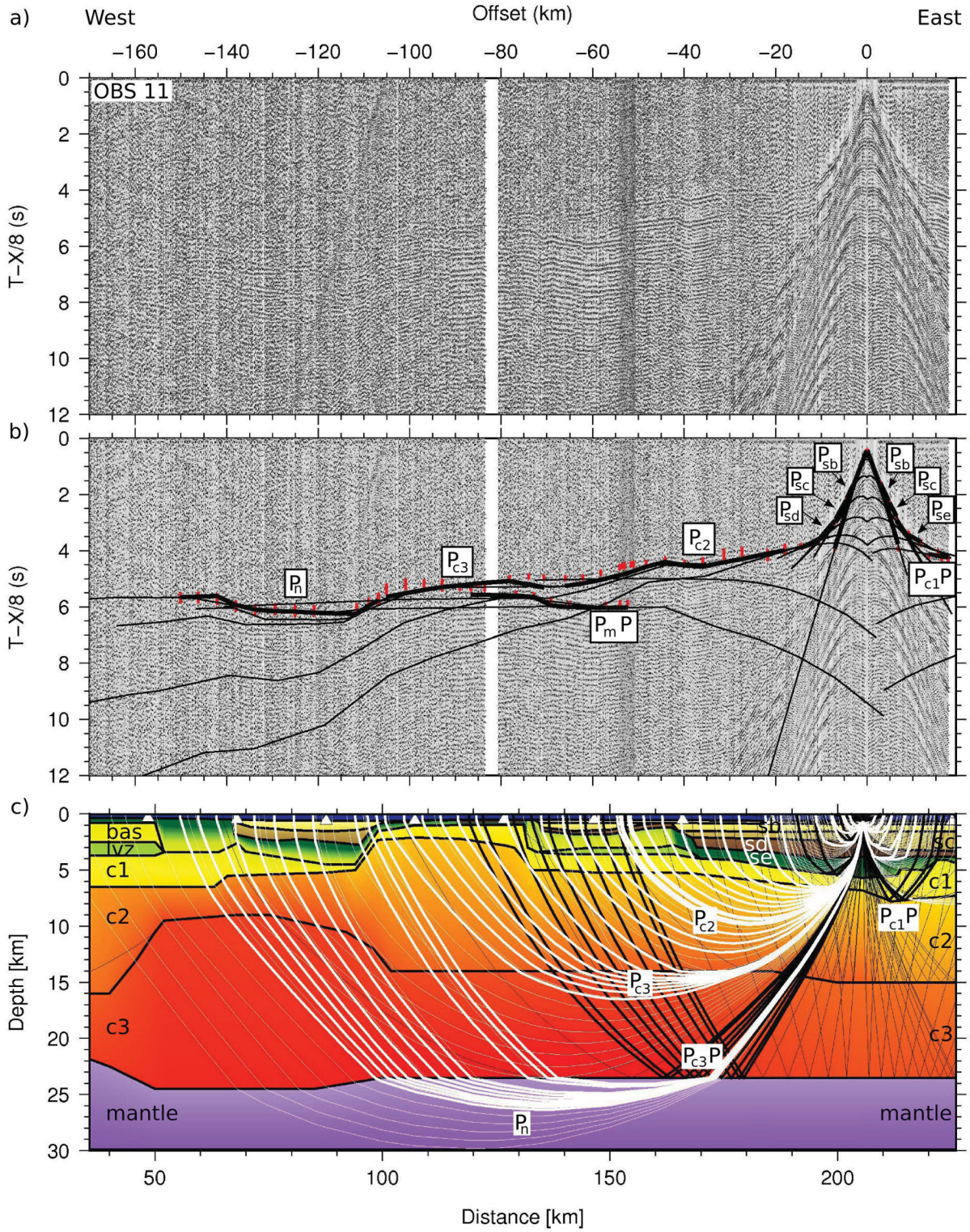

Figure 7. (a) Seismic section of OBS 11, displayed with a reduction velocity of 8 km s^{-1}. (b) The same seismic section with picks in red; the pick length corresponds to the assigned pick uncertainty; calculated traveltimes are displayed in black with thick black lines corresponding to the picks. (c) *P*-wave velocity model with ray paths. Model layers are annotated; black rays indicate reflected phases, white rays refracted phases; thick lines correspond to the picks in the central panel.

of how well the calculated traveltimes are within the range of the assigned pick uncertainties and should ideally be 1. The normalized χ^2 of our model is 1.965, which is almost twice the ideal value. But a comparison with the *P*-wave velocity models of Mackenzie *et al.* (2005) (χ^2 of 2.563) and Voss & Jokat (2007) (χ^2 of 2.804 and of 3.049) shows that χ^2 values greater than 2 are not uncommon. The RMS error of our model is 177 ms, which is higher than the values of the before mentioned publications, which range from 137

Table 5. Corrections applied to the gravity data.

– time shift due to overcritical damping of the sensor
– conversion from instrument reading units to mGal
– tie to world gravity net IGSN 71 with connection measurements
– correction for the Eötvös effect with navigation data
– correction for instrument drift during the cruise
– subtraction of normal gravity (GRS80)

to 164 ms. Especially phases from the lower crust contribute to the high RMS error. We think that the high RMS error is mainly due to the low signal to noise ratio of the OBS data. The model depicts a complex crust, which various vertical features where scattering of the deep phases can lower the signal amplitudes. Fig. 3 shows the diagonal values of the resolution matrix as a colour grid. The resolution is a measure of how well a velocity value is constrained by all rays passing though it. The layers of the model are over all well resolved, except for the profile terminations.

5 GRAVITY AND MAGNETIC ANOMALY DATA

For free-air gravity anomalies, standard processing steps as listed in Table 5 were applied to the gravity data. We obtained a density model by forward modelling with the software GM-SYS (Geosoft, Inc.). For the starting model (Fig. 8c), we used a simplified geometry of the *P*-wave velocity model. Line AWI-20080700 of the *P*-wave velocity model only extends up to a model distance of 226 km, while gravity data were recorded on line BGR08-301 up to a model distance of 315 km. Density values were derived from average *P*-wave velocities according to (Barton 1986). For simplicity, we combined the upper three sediment layers with *P*-wave velocities of 1.7–2.9 km s^{-1} to one density body of 2200 kg/m^3 (s1). The two underlying layers of 3.1–5.6 km s^{-1} are combined to one layer of 2450 kg m^{-3} density (s2). The basalt flow from a model distance of 35–50 km is added to the first crustal layer. We used the basement interpretation of the MCS data along the whole density model (Figs 2 and 8).

Calculated free-air gravity values of the starting model are generally too high along the western part of the profile and too low at the eastern part (Fig. 8b). We therefore divided the mantle at a model distance of 170 km into a body of 3200 and 3300 kg m^{-3}. Where this density change was not sufficient, we adjusted the layer boundaries. From a model distance of 117–135 km, we replaced the second sediment layer (2450 kg m^{-3}) by the first (2200 kg m^{-3}), to meet smaller free-air gravity values in this region. This density change is also indicated by a lateral change in *P*-wave velocities (4.8–4.1 km s^{-1}) along line AWI-20080700. Further, we adjusted the crustal layers east of a model distance of 225 km. This area is not covered by the *P*-wave velocity model, so only the depth of the basement is constrained by the MCS data. To fit the high free-air gravity values east of 270 km, we modelled a shallowing of the middle and lower crust.

The average difference between the calculated gravity of the final model (Fig. 8d) and the observed free-air gravity values is 7.2 mGal, in contrast to 40.5 mGal for the starting model. The greatest mismatches between modelled and observed gravity occur at model distances of 0–65 km and 110–150 km. These regions are in the vicinity of strong positive anomalies off the profile (Fig. 1b) and we therefore interpret these as the influence of 3-D effects.

To obtain residual magnetic anomaly values, the appropriate IGRF reference field values (IGRF-10) were removed from the measured magnetic total intensity. It was necessary to add 100 nT to the anomaly curve to meet the mean level of two published magnetic maps (Verhoef *et al.* 1996; Maus *et al.* 2009). The magnetic anomalies (Fig. 8a) vary between positive and negative values of −1146 nT (at a model distance of 32 km) and 1015 nT (47 km). In general, magnetic anomalies have small amplitudes and long wavelengths at the locations of sedimentary basins (at model distances of 68–100 km and east of 135 km) and high amplitudes with small wavelengths where the basement is near the surface.

6 PLATE KINEMATICS

We use GPlates (www.gplates.org) to visualize the tectonic evolution of the Davis Strait area. For the relative motion of the Greenland plate to the North American craton, we use the set of rotation poles by Oakey (2005). This recent reconstruction complements the previous reconstruction from Roest & Srivastava (1989). The most relevant time steps in the tectonic evolution of the Davis Strait, as illustrated in Fig. 9, are:

90 Ma: Greenland separates from Canada in an eastwards direction; rifting is active, but seafloor spreading has not started in the Labrador Sea (Roest & Srivastava 1989; Chalmers & Laursen 1995).

57 Ma: Greenland and Canada are at a maximum east-west distance in the Davis Strait; the motion of Greenland changes from an eastward to a northeastward direction (Srivastava 1978); seafloor spreading is active in the Labrador Sea (Srivastava 1978; Chalmers & Laursen 1995).

33 Ma: Seafloor spreading ceases in the Labrador Sea (Srivastava 1978); Greenland and Canada are placed at their modern configuration.

Between 57 and 33 Ma, Greenland moved northwards by 310 km relative to the North American craton. This resulted in a narrowing of the central Davis Strait. If we use the location of the Hudson Fracture Zone as shown in Chalmers & Pulvertaft (2001) for the plate boundary, pure strike-slip motion occurs along this fault (Fig. 9e). If we use the location of the Ungava Fault Complex instead, a crustal overlap of 70 km width must be compensated. The area of this overlap coincides with the positive free-air gravity anomalies that are associated with the Ungava Fault Complex. This is the area where transpressional forces were compensated.

7 DISCUSSION

7.1 Basalts and sediments

Below the sediment packages **sc** and **sd**, we modelled a layer **se** (Fig. 3). This layer with *P*-wave velocities of 4.1–5.1 km s^{-1} is similar to a layer with *P*-wave velocities of 4.3–5.3 km s^{-1}, observed on NUGGET-1 (Funck *et al.* 2007). This layer was drilled at the Hekja O-71 and the Gjoa G-37 wells (Fig. 1a) and consists of basalts intercalated with sediments (Klose *et al.* 1982). Due to the similarity of the *P*-wave velocity character and the proximity to NUGGET-1, we follow this interpretation for line AWI-20080700/BGR08-301.

At a model distance of 55–68 km, dipping reflectors in the MCS data confirm this interpretation (basalt flows in closeup A in Fig. 2). High amplitudes and frequencies of the magnetic anomaly data also support the interpretation of volcanics near the surface (Fig. 8a).

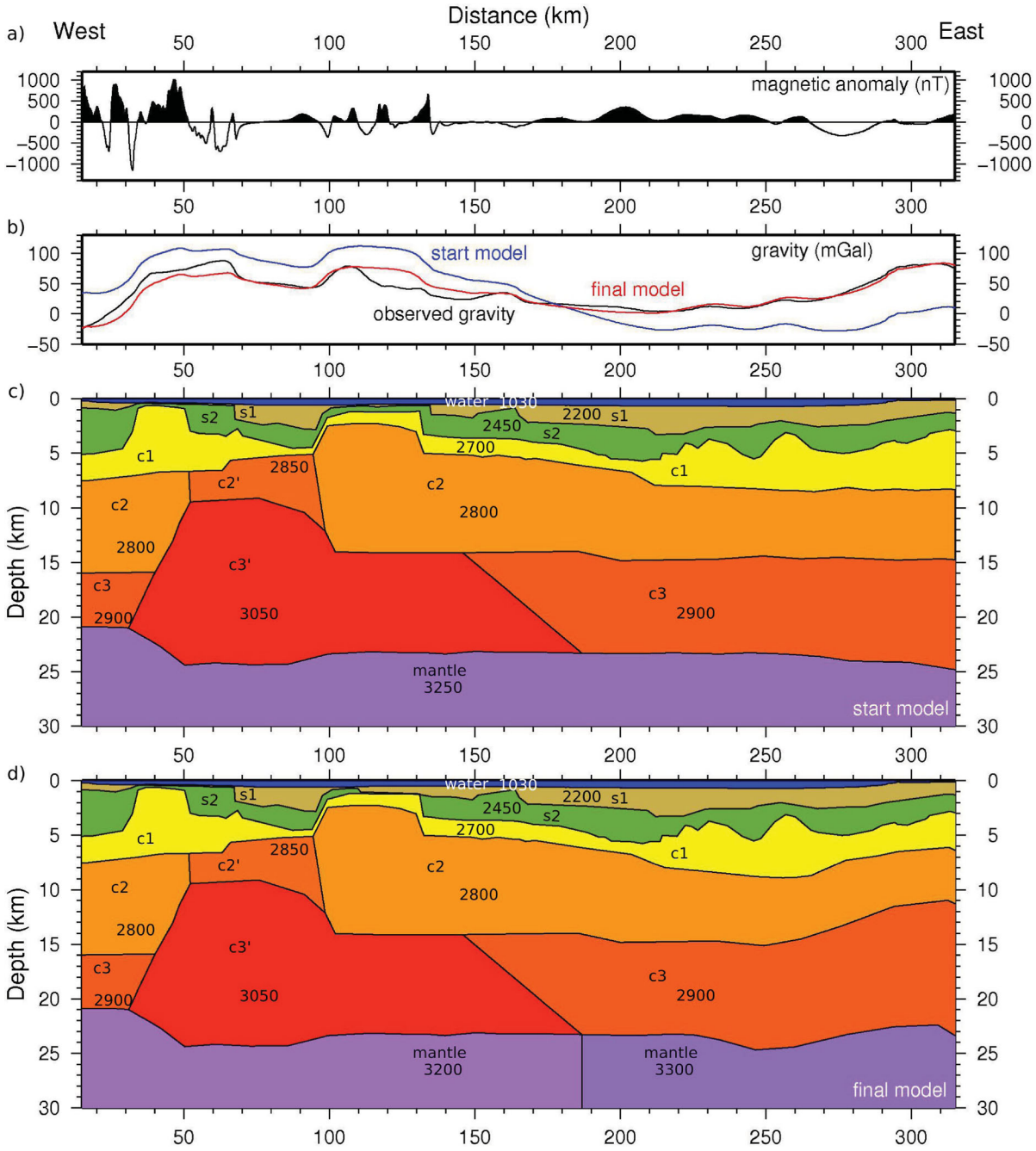

Figure 8. (a) Magnetic anomaly data along line BGR08-301. (b) Free-air gravity data along line BGR08-301. Observed gravity in black, calculated gravity of the start model in blue (c), of the final model in red (d). (c) Start model of the density modelling; layer boundaries are taken from the *P*-wave velocity model and average *P*-wave velocities are transferred to densities according to Barton (1986). Numbers inside the model indicate densities in kg m^{-3}. (d) Final density model.

The only indication of the separately modelled body **bas** with *P*-wave velocities of 5.4 km s^{-1} in the MCS data is an undulation of the basement at a modal distance of 38 km (Fig. 2). It is confirmed by the density model, where it is modelled with the same density as the upper crust (model distance 35–50 km). Due to this high density, we interpret this feature as a separate basalt unit, which is not intercalated with sediments. Model distances 0–50 km are underlain by a LVZ, which we interpret as sediments that were covered by the basalt unit (Fig. 10).

From a model distance of 95–130 km, the layer **se** is much thinner than modelled to the west (0.5 km instead of 2 km). High amplitudes and frequencies of the magnetic anomaly data indicate that volcanics are near the surface (Fig. 8a). From the available data, it is not clear whether this sequence was deposited on this basement high with only 0.5 km thickness, or if it was deposited before an uplift of the basement with 2 km thickness like in the west. In the later case, 1.5 km of it were eroded due to uplift and exposure at the seafloor. *P*-wave velocities of 4.8 km s^{-1} from a model distance of 95–117 km

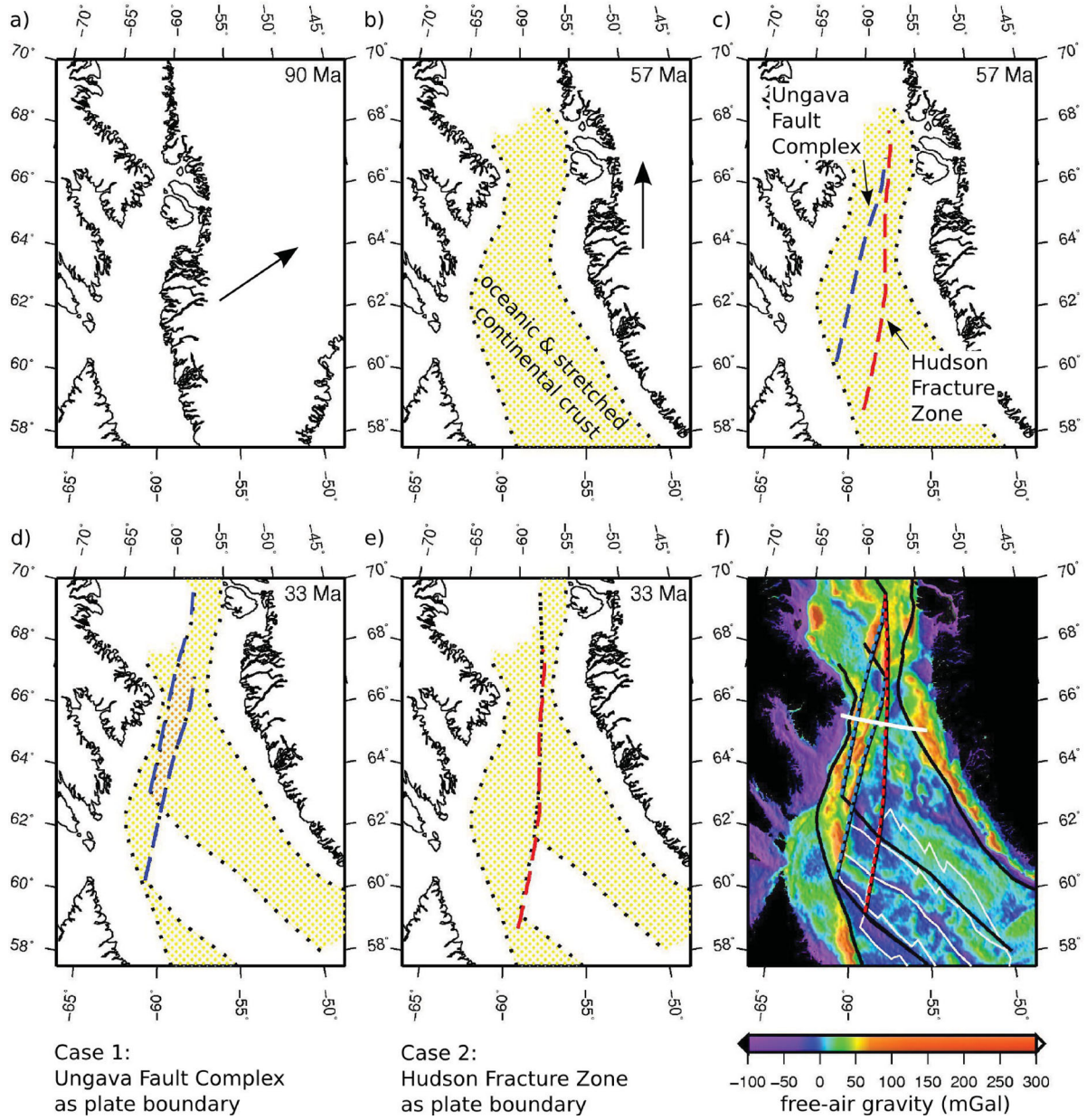

Figure 9. Tectonic evolution of the Davis Strait with poles of rotation from Oakey (2005). (a) Configuration at 90 Ma. (b) and (c) The maximum east–west separation of the North American craton and Greenland is reached at 57 Ma. The area of additional crust relative to 90 Ma (stretched continental and oceanic crust) is shaded in yellow; the location of the Ungava Fault Complex and the Hudson Fracture Zone are marked. (Lower row) Relative motion between Greenland and Canada terminates at 33 Ma; the plates are at their present day configuration. (d) Case 1: The Ungava Fault Complex is used as a plate boundary; due to the northward motion of Greenland, an overlap of crust needs to be compensated (shaded in orange). (e) Case 2: The Hudson Fracture Zone is used as a plate boundary; only strike-slip motion is active without thickening or thinning of the crust. (f) Free-air gravity anomalies (Sandwell & Smith 2009), version 18.1, with the outline of overlapping crust, the Ungava Fault Complex in blue, the Hudson Fracture Zone in red, and oceanic crust in the Labrador Sea as outlined by Chalmers & Pulvertaft (2001) in white; line AWI-20080700/BGR08-301 in the Davis Strait as thick white line.

support this interpretation as do dipping reflectors in the MCS data (Figs 2 and 11). A graben structure of the interpreted basement separates this section from lower *P*-wave velocities (4.1 km s^{-1}) and densities (2450–2200 kg m^{-3}) from a model distance of 117–130 km (Fig. 11). As *P*-wave velocities of basalts can range between 3.5 and 6.5 km s^{-1} due to varying composition and deposition (Christie *et al.* 2006), we here also interpret layer **se** as basalts intercalated with sediments.

From a model distance of 130–165 km, high-amplitude reflections of low frequency line up in the MCS data (Fig. 2 with closeup B). The reflection pattern is similar to drilled volcanics in the vicinity of the Gjoa G-37 well (fig. 9 in Klose *et al.* 1982). The *P*-wave velocity of 5.0 km s^{-1} is also within the range for basalts (Christie *et al.* 2006). This section is underlain by a LVZ, which represents old sediments that were covered by the basalt flows.

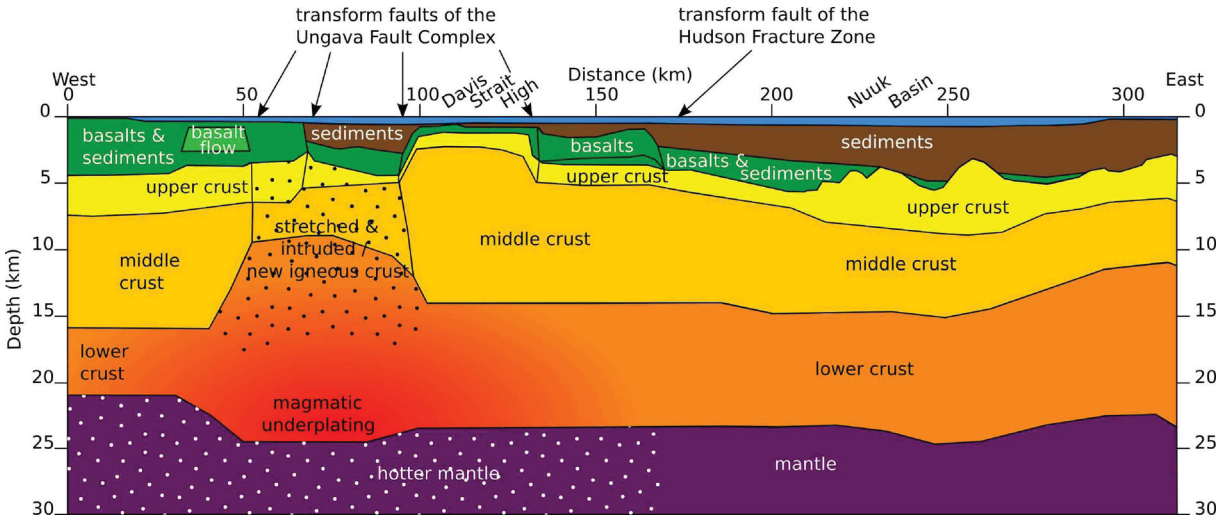

Figure 10. Geological structure of line AWI-20080700/BGR08-301 compiled from the MCS data (Fig. 2), the *P*-wave velocity and the density models (Figs 3 and 8).

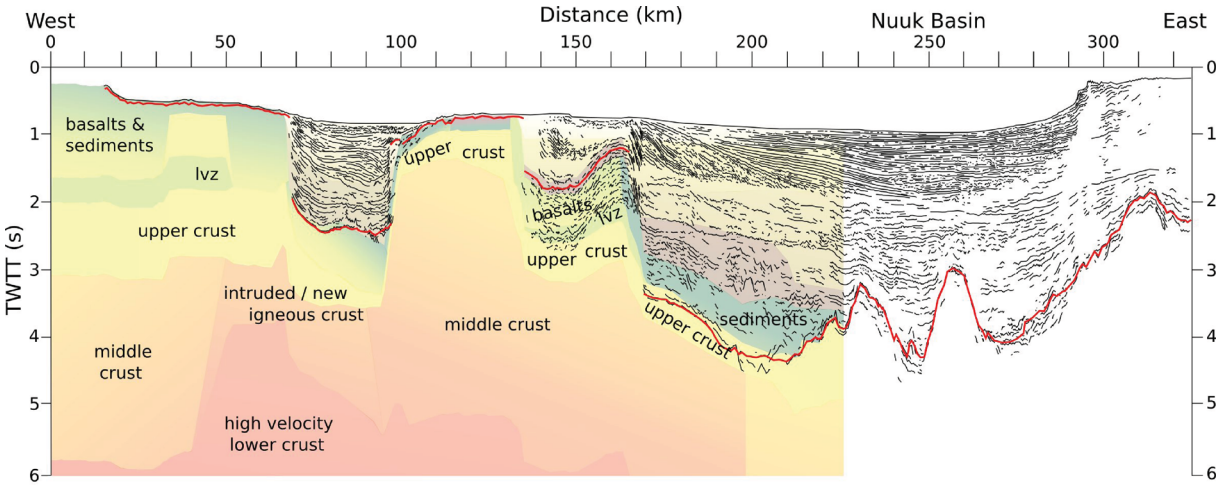

Figure 11. Line drawing of the MCS data of line BGR08-301 overlain with the time-converted *P*-wave velocity model from Fig. 3.

East of a model distance of 165 km, in the Nuuk Basin (Fig. 1b), *P*-wave velocities of layer **se** are only 4.6 km s^{-1} (Fig. 3). This is the only part of the profile, where we interpreted the lower boundary of this layer as basement instead of the upper boundary. The top of layer **se** causes a high-amplitude continuous reflection in the MCS data from a model distance of 165–190 km (Fig. 2). This is similar to reflections of the top of basalts from a model distance of 140–165 km. From 165 to 230 km, the upper boundary of layer **se** is characterized by diffuse reflections, which can indicate a broken surface (Fig. 2). Although *P*-wave velocities of layer **se** are lower in the Nuuk Basin than along the rest of the model, we here also interpret basalt flows due to the high-amplitude reflections in the MCS data (Fig. 10).

7.2 Crustal structure

The *P*-wave velocity and density model consist of a three layered crusts: the upper, middle, and lower crust. While the *P*-wave velocity and density structure of the upper crust is uniform along the profile, the middle crust is characterized by higher *P*-wave velocities and densities from a model distance of 50–95 km, like the lower crust between 40 and 170 km. A lateral change was also modelled in the mantle with smaller densities west of a model distance of 170 km.

7.2.1 Stretched and highly intruded/igneous crust, model distance: 50–95 km

The higher *P*-wave velocities and densities of the middle and lower crust at a model distance of 40–100 km show an increased content of mafic material. This can be in the form of mafic intrusions in a stretched and fractured continental crust, or in the form of newly formed oceanic crust. The following paragraphs discuss both options.

The average thickness of normal oceanic crust is 7.1 ± 0.8 km and of plume affected oceanic crust is 10.3 ± 1.7 km (White *et al.* 1992). This is only half of the crustal thickness of our model. From the top of layer **c1** to the base of layer **c3** we measure 20 km thickness. Oceanic crust of a similar thickness is reported at oceanic plateaus as parts of large igneous provinces. Gohl & Uenzelmann-Neben (2001) report that a 17-km-thick high-velocity lower crust (*P*-wave

velocities of 7.0–7.5 km s^{-1}) overlains by a 3-km-thick layer of *P*-wave velocities of 6.5–6.8 km s^{-1} at the Agulhas Plateau. This crustal structure is similar to the model of line AWI-20080700 with *P*-wave velocities of 6.9–7.3 km s^{-1} in a 15-km-thick lower crust and 6.3–6.9 km s^{-1} in a 3.5-km-thick middle crust. Therefore, an interpretation of new igneous crust from the *P*-wave velocities is possible.

Other locations of thick oceanic crust are the volcanic continental margins of East Greenland (Holbrook *et al.* 2001; Hopper *et al.* 2003) (more than 30 km thickness to 18.3 km thickness depending on the distance to the Iceland hotspot track) and the Vøring Plateau (Mjelde *et al.* 2005) (23.5–9 km thickness). Like the Davis Strait area, both locations were influenced by the Iceland mantle plume, with production of thick basalt flows during the breakup process (Storey *et al.* 1998; Holbrook *et al.* 2001; Hopper *et al.* 2003; Mjelde *et al.* 2005). Basalt flows are also present along AWI-20080700/BGR08-301 with varying thickness. The basalts from a model distance of 0–68 km are part of the seaward dipping reflectors at the Baffin Island margin reported by Skaarup *et al.* (2006).

A difference to the East Greenland margin and the Vøring Plateau is the moderate *P*-wave velocities in the middle and lower crust. Along AWI-20080700, the middle crust is 3.5 km thick with an average *P*-wave velocity of 6.6 km s^{-1} and the lower crust is 14 km thick with an average *P*-wave velocity of 7.1 km s^{-1}. Hopper *et al.* (2003) model a crust with 6.6 km s^{-1} at the top and 7.5 km s^{-1} at the base. *P*-wave velocity models of the East Greenland margin shown in Holbrook *et al.* (2001) exceed 7.5 km s^{-1} in the lower crust. Mjelde *et al.* (2005) model a layer of 6.8, 7.1 and 7.3 km s^{-1}. It is therefore likely that the crust along AWI-20080700 does not consist completely of new igneous material, but of highly intruded continental crust. According to Rudnick & Fountain (1995), the middle crust of rifted margins is 7.5 ± 5.6 km thick with an average *P*-wave velocity of 6.4 ± 0.3 km s^{-1}; the lower crust is 8.6 ± 5.1 km thick with a *P*-wave velocity of 7.0 ± 0.3 km s^{-1}. Although rifted margins vary greatly, these global averages fit well to the layers of our model (see above). This interpretation requires that the basalt flows along the model are not products of a breakup, but that they are related to volcanism along fractures of the Ungava Fault Complex.

Other methods that are used to identify oceanic crust are magnetic spreading anomalies and the basement morphology. Because of the small scales (45 km of crust), no magnetic seafloor spreading anomalies can be expected. The basement morphology is only visible below the sedimentary basin from a model distance of 68–95 km in the MCS data. But it cannot distinguished between a basalt covered continental crust and newly formed oceanic crust.

As we cannot rule out either interpretation, we refer to the crust between a model distance of 50–95 km as stretched and intruded/igneous crust in the following (Fig. 10).

We compare the crustal model along line AWI-20080700/BGR08-301 to that of NUGGET-1 (Funck *et al.* 2007). Along both profiles, the continental crust of Baffin Island and Greenland is separated by thin crust with a high content of mafic material. On NUGGET-1, Funck *et al.* (2007) modelled a 140-km-long section of oceanic layers 2 (5.4–6.2 km s^{-1}) and 3 (6.7–7.0 km s^{-1}) underlain by a thick magmatic underplating of *P*-wave velocities of 7.4 km s^{-1}. On NUGGET-1 and AWI-20080700/BGR08-301, this crust is divided into a western and an eastern section. On line AWI-20080700/BGR08-301 at a model distance of 68 km, the upper crust thins by 1.5 km and rises. The western part, from a model distance of 50–68 km, is covered by a thick succession of basalts intercalated with sediments. The eastern part, from 68–100 km, is also covered by basalts and by a sedimentary basin. On NUGGET-1, a graben structure filled with basalts divides the western and eastern section. We interpret the sharp boundary between the eastern and western segment of intruded/igneous crust as a transform fault of the Ungava Fault Complex.

Funck *et al.* (2007) propose that the western part of the oceanic crust is related to the volcanic type margin of Baffin Island and Labrador. We expand this interpretation to line AWI-20080700/BGR08-301, as we also imaged basalt flows at the western end of our profile in the models, the MCS and the magnetic anomaly data (Figs 2, 3 and 8). These volcanics, southeast of Cape Dyer, are partly exposed at the seafloor and are mapped by Skaarup *et al.* (2006) from seismic reflection lines and potential field data.

Funck *et al.* (2007) further describe the evolution of oceanic crust at the eastern segment as an upwelling of magma in areas of transtensional movement along the Ungava Fault Complex. From the plate kinematic reconstruction (Fig. 9), we know that in the period between 57 and 33 Ma, strike-slip motion and compression were active in the Davis Strait. The stretched crust must therefore have evolved prior to 57 Ma when the strait was opening. The intruded/igneous crust along line AWI-20080700/BGR08-301 and the oceanic crust along NUGGET-1 (Funck *et al.* 2007) are both in line with gravity anomalies of the Ungava Fault Complex. We therefore propose that stretched and intruded crust/oceanic crust is present between both lines along the Ungava Fault Complex. The location of the Ungava Fault Complex therefore marks the plate boundary between Baffin Island and Greenland prior to 57 Ma.

7.2.2 High-velocity lower crust

P-wave velocities of the lower crust higher than 7.0 km s^{-1} are often interpreted as magmatic underplating (Furlong & Fountain 1986; Marillier & Reid 1990). Underplating has also been reported on the nearby lines GR89-WA (Gohl & Smithson 1993) and NUGGET-1 and -2 (Funck *et al.* 2007; Gerlings *et al.* 2009) in Fig. 1. *P*-wave velocities of these magmatic underplatings are higher than the velocities we have modelled on line AWI-20080700 (in the range of 7.4–7.7 km s^{-1} instead of 6.9–7.4 km s^{-1}). As there is no boundary detected between lower crust and an underplated body, we interpret a gradual increase of mafic material from the sides to the centre of the model. The thickening of the lower crust from a model distance of 30–100 km shows that mafic material was added to the lower crust. This is similar to the interpretation of a magmatic underplating along other profiles (GR89-WA (Gohl & Smithson 1993), NUGGET-1 (Funck *et al.* 2007) and NUGGET-2 (Gerlings *et al.* 2009)).

Lower mantle densities in the free-air gravity model indicate that the high-velocity lower crust is underlain by a hotter mantle than the eastern part of line AWI-20080700/BGR08-301. The high content of mafic material in the centre of the models can be the result of decompressional mantle melts during extension of the lithosphere (McKenzie & Bickle 1988) and/or due to the influence of a mantle plume (White & McKenzie 1989).

Funck *et al.* (2007) relate the magmatic underplating along NUGGET line 1 to the Greenland–Iceland mantle plume. Volcanics of Disco Island are dated to 61 Ma and have been related to the Iceland plume (Storey *et al.* 1998). Funck *et al.* (2007) suggest that according to the hypothesis of Sleep (1997), buoyant plume mate-

rial flowed southwards along thin lithosphere in the central Davis Strait. Although we cannot confirm the origin of the mafic material along line AWI-20080700/BGR08-301, it supports the hypothesis of Funck *et al.* (2007) that material of the Iceland plume was channelled southwards along thinned lithosphere in the Davis Strait.

7.2.3 Continental crust, model distance: 0–50 and 95–315 km

We interpret the crust, west of a model distance of 40 km and east of a model distance of 100 km, as rifted continental crust according to the *P*-wave velocity compilation from Rudnick & Fountain (1995) and the thickness of up to 19 km.

The section from a model distance of 95–135 km is the Davis Strait High, which crops out farther north. Although the Davis Strait area was a rifting system prior to 57 Ma (see Section 6), the Davis Strait High is elevated to seafloor level instead of having subsided. As Chalmers & Pulvertaft (2001) have proposed, this indicates that compressional forces within the Ungava Fault Complex caused an uplift of continental crust. We suggest that the presence of buoyant plume material has supported this uplift.

Steps in the basement morphology indicate faults at a model distance of 68, 95, 135 and 165 km (Fig. 2). From the *P*-wave velocity and density model, we introduced an additional fault at the western border of continental to intruded/igneous crust at a model distance of 50 km. The faults from a model distance of 50–135 km are within the transform fault system of the Ungava Fault Complex (Sørensen 2006) and we therefore interpret them as transform faults with a normal component (Fig. 10). The fault at 165 km lies at the location of the Hudson Fracture Zone (Chalmers & Pulvertaft 2001), which is also a transform fault with a normal component. The continental crust is broken into several segments that have been uplifted relative to one another and were transported along transform faults of the Ungava Fault Complex and the Hudson Fracture Zone.

Model distance 0–50 km: Stretched continental crust of 6–16 km thickness, divided into upper, middle and lower crust, covered by basalts intercalated with sediments.

Model distance 50–95 km: Stretched and intruded crust or new igneous crust with a high-velocity mafic lower crust, covered by basalts intercalated with sediments and partly by a sediment basin.

Model distance 95–226 km: Stretched continental crust of 12–19 km thickness, with a high-velocity lower crust merging into less intruded lower crust from west to east, covered by sediments and partly by basalt flows.

7.3 Ungava Fault Complex and Hudson Fracture Zone

Transform faults of the Ungava Fault Complex are recently derived by Sørensen (2006) from Bouguer gravity data. Our new models and data offer new constraints on the location of these faults. We use regional magnetic anomaly and satellite-derived gravity data to extend the faults perpendicular to our profile (Fig. 12).

The fault at a model distance of 95 km separates intruded/igneous crust from the Davis Strait High and matches exactly the location that Sørensen (2006) proposes (Fig. 12). On our line, the eastern border of the Davis Strait High lies 14 km east of the location from Sørensen (2006). We also propose a more north–south striking trend from the gravity data. The fault that bounds the crust of the Nuuk Basin to the west (at a model distance of 170 km) is not mapped by Sørensen (2006). It lies on the Hudson Fracture Zone, which is a north–south striking fault (Srivastava 1978; Chalmers & Pulvertaft 2001), that is not clearly imaged by the regional potential field data. While the eastern boundary of the intruded/igneous crust coincides well with the existing fault map, the western boundary needs to be shifted eastwards by 40 km. The north–south extent of this fault is well indicated by a polarity change in the magnetic anomaly data (our interpretation in Fig. 12b). Furthermore, the fault within the intruded/igneous crust is well marked by a polarity change. On our profile, this fault had to be shifted 14 km eastwards relative to the Sørensen (2006) interpretation.

To determine the role of the Ungava Fault Complex and the Hudson Fracture Zone in the time between 57–33 Ma, we develop two-plate tectonic end-member models:

In the first case, we use the Ungava Fault Complex as a plate boundary and neglect the Hudson Fracture Zone: Although transform forces dominate the Ungava Fault Complex, compressional forces also occur and must compensate overlapping crust of 70 km width (Fig. 9d). Evidence for compression is the varying thickness of the crust along our line. The middle crust of the Davis Strait High is, for example, 2.5 km thicker than that of the adjacent eastern crust (at a model distance of 140–170 km). This can be due to compression. However, these units may have been transported to their present position along the Greenland margin via transform faults of the Ungava Fault Complex, and thus the crustal thickness does not need to be equal. If a deformation in the scale of 70 km has occurred, this should also affect the pre-Eocene sediments that directly overly the basement. Deformed sediments are present at a model distance of 140–170 km (east the Davis Strait High, closeup B in Fig. 2). Balancing the bulged sediments only leads to a lateral extension of 0.5 km, which is far from the expected value of 70 km. On the Davis Strait High, there is no sediment cover detected, which could verify deformations. We conclude that our models image transform faults of the Ungava Fault Complex dividing the crust, but compression can only have occurred in a scale of a few kilometres.

In the second case, we use the Hudson Fracture Zone as a plate boundary and neglect the Ungava Fault Complex: No compressional forces occur in the Davis Strait area, only strike-slip motion along the Hudson Fracture Zone connects the opening of the Labrador Sea and the Baffin Bay (Fig. 9e). Although this model fits the plate kinematics and the sediment record, some motion must have occurred along the Ungava Fault Complex which is clearly imaged by the data we here present and by the regional potential field data.

Given that the poles of rotation from (Oakey 2005) are correct, the Ungava Fault Complex and the Hudson Fracture Zone must have been active in the Davis Strait area. We propose that a change took place from transpression along the Ungava Fault Complex to strike-slip motion along the Hudson Fracture zone. Prior to 57 Ma, Davis Strait was opening and highly stretched and intruded continental crust (line AWI-20080700/BGR08-301) or oceanic-type crust (NUGGET-1, Funck *et al.* (2007)) evolved within the location of the Ungava Fault Complex, which marks the plate boundary at that time. When the Greenland motion relative to the North American craton changed to a more northward direction at 57 Ma, transpression along the Ungava Fault Complex was active as a result of its relative weak lithosphere. As the northward motion of Greenland continued, the stress was no longer compensated by the deformation of crust within the Ungava Fault Complex, but the Hudson Fracture Zone evolved with pure strike-slip motion. Although the Hudson

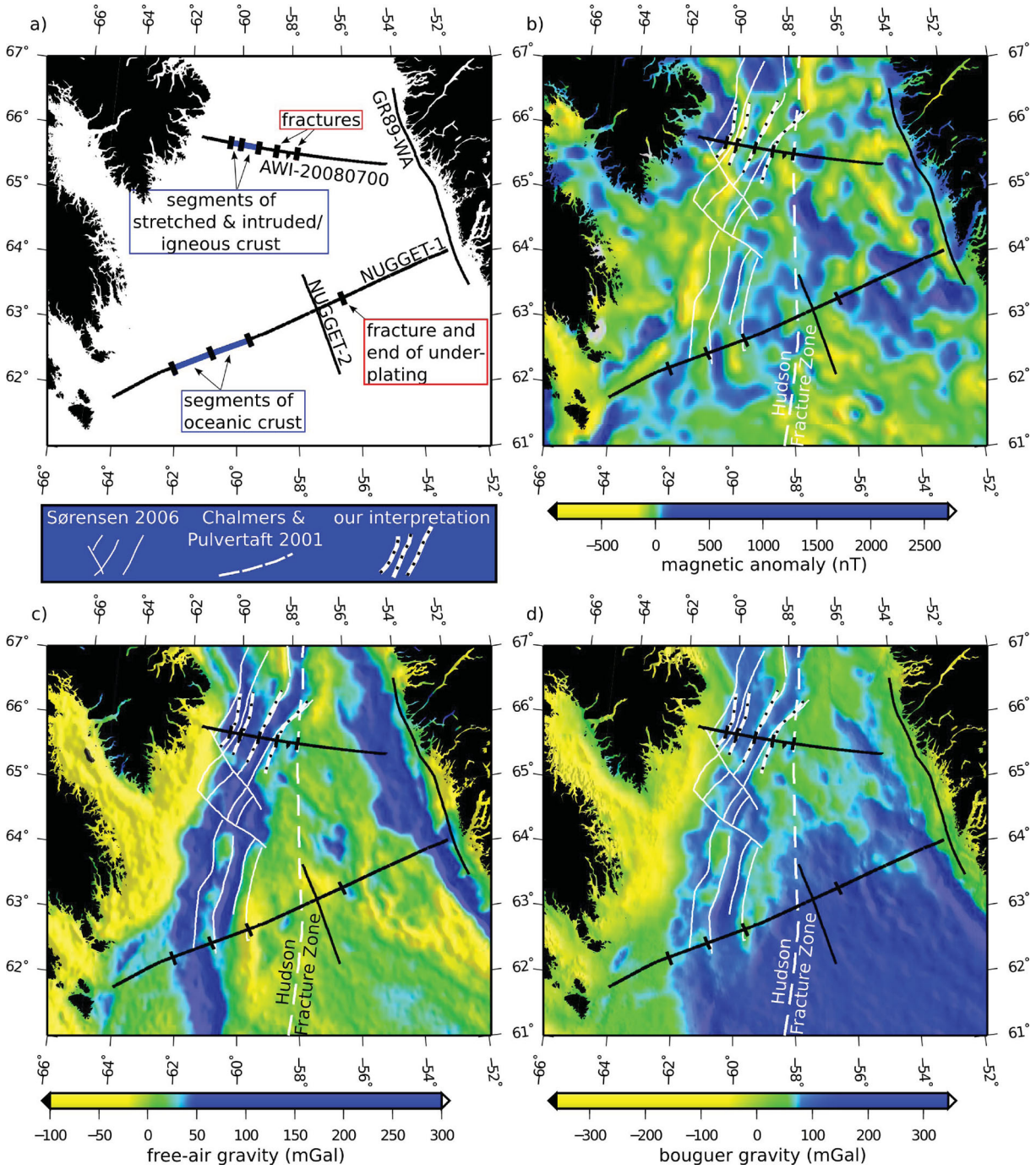

Figure 12. (a) Locations of seismic refraction lines (AWI-20080700, GR89-WA (Gohl & Smithson 1993), NUGGET-1 (Funck *et al.* 2007), NUGGET-2 (Gerlings *et al.* 2009)). On the profiles, fractures and interpretations are marked. (b) Magnetic anomaly data (EMAG2 V2, Maus *et al.* (2009)) overlain with the same data as in the upper left panel. Locations of faults of the Ungava Fault Complex after Sørensen (2006), the location of the Hudson Fracture Zone after Chalmers & Pulvertaft (2001) and our interpretation are marked. (c) Satellite-derived free-air gravity anomalies ((Sandwell & Smith 2009), version 18.1) overlain with the same information as in the upper right panel. (d) Bouguer gravity anomalies reduced to sea level (DNSC08 free-air gravity data (Andersen *et al.* 2008) and Smith & Sandwell (1997) topography, version 13.1, used with code from Fullea *et al.* 2008) overlain with the same information as in the upper right panel.

Fracture Zone is not well imaged by the regional gravity data and has thus often been neglected in the literature, it likely compensated most of the relative motion between the North American craton and Greenland. As the crust along the Hudson Fracture Zone was not deformed with respect to its thickness, it is not indicated by the regional gravity data.

8 CONCLUSIONS

To determine the nature of the central Davis Strait crust, we developed a *P*-wave velocity and a density model, and interpret these with additional seismic reflection and magnetic anomaly data (Figs. 2, 3 and 8). The profile is dominated by continental crust that is

separated by a 45-km-long section of stretched and intruded/new igneous crust (Fig. 10). It is similar in the *P*-wave velocity and density structure to oceanic crust along NUGGET-1 in the northern Labrador Sea, Fig. 1 (Funck *et al.* 2007). On both profiles, this section is divided into an eastern and a western segment by a transform fault of the Ungava Fault Complex. We suggest that oceanic crust/stretched and intruded crust is also present between both lines and follows the gravity anomalies that mark the Ungava Fault Complex (Figs 12c and d). Beneath the intruded/igneous crust lies a thick high-velocity lower crust (Fig. 10) that can be related to the Iceland plume which influenced the Davis Strait region in the Paleocene (Lawver & Müller 1994; Storey *et al.* 1998). We infer that buoyant plume material was channelled southwards along thinned lithosphere in the Davis Strait and formed a zone of magmatic underplating in the northern Labrador Sea. Resulting volcanic activity along the Baffin Island margin is also indicated by basalts flows along our profile (Fig. 2).

The Davis Strait is dominated by the transform fault system of the Ungava Fault Complex and the Hudson Fracture Zone. We analysed the role of both fault systems for the Davis Strait area with plate kinematic modelling (Fig. 9). While the Davis Strait was opening prior to 57 Ma, stretched and intruded crust evolved along the location of the Ungava Fault Complex, which was the plate boundary at that time. When the Greenland motion changed to a more northward component, transpressional motion had to be compensated and the Ungava Fault Complex evolved. Crust was deformed and transported along transform faults. At some point, compressional deformation of the crust caused more stress than could be compensated and the Hudson Fracture Zone with pure strike-slip motion evolved. As this transform fault is not accompanied by crustal thickening or thinning, it is not well represented by the regional potential field data and has thus not been recognized to the same extent as the Ungava Fault Complex has. As we only find evidence of minor compression along our profile, most of the motion between the North American plate and Greenland at 57–33 Ma must have taken place along the Hudson Fracture Zone.

ACKNOWLEDGMENTS

We thank the master and crew of RV Merian for their support during the cruise. For processing of the MCS data, we thank Ewald Lüschen. Tabea Altenbernd, Martin Block and Sonja Breuer contributed in several discussions to the interpretation of the MCS data. For providing the OBS to TF via an EU grant in 2008 (contract RITA-CT-2004505311), we acknowledge Ernst Flüh from Geomar. We thank the German Research Council DFG for funding the cruise MSM09/3. The data analysis and study was financed by institutional funds of AWI and BGR. We also thank two anonymous reviewers for improving the manuscript.

REFERENCES

Andersen, O., Knudsen, P., Berry, P. & Kenyon, S., 2008. The DNSC08 ocean wide altimetry derived gravity anomaly field, talk, EGU-2008, Vienna, Austria.

Barton, P., 1986. The relationship between seismic velocity and density in continental crust - a useful constraint?, *Geophys. J. R. astr. Soc.,* **87,** 195–208.

Chalmers, J. & Laursen, K., 1995. Labrador Sea: the extent of continental and oceanic crust and the timing of the onset of seafloor spreading, *Mar. Pet. Geol.,* **12,** 205–217.

Chalmers, J. & Pulvertaft, T., 2001. Development of continental margins of the Labrador Sea: a review, in *Non-Volcanic Rifting of Continental Margins: A Comparison of Evidence from Land and Sea,* Vol. 187, pp. 77–105, eds Wilson, R., Whitmarsh, R., Taylor, B. & Froitzheim, N., Geol. Soc. London.

Chalmers, J., Pulvertaft, T., Marcussen, C. & Pedersen, A., 1999. New insight into the structure of the Nuussuaq Basin, central West Greenland, *Mar. Pet. Geol.,* **16,** 197–224.

Christie, P., Gollifer, I. & Cowper, D., 2006. Borehole seismic studies of volcanic succession from the Lopra-1/1a borehole in the Faroe Islands, northern North Atlantic, *Geol. Surv. Denmark Greenland Bull.,* **9,** 23–40.

Clarke, D. & Upton, B., 1971. Tertiary basalts of Baffin Island: field relations and tectonic setting, *Can. J. Earth Sci.,* **8**(248), 248–258.

Dalhoff, F. *et al.*, 2006. Continental crust in the Davis Strait: new evidence from seabed sampling, *Geol. Surv. Denmark Greenland Bull.,* **10,** 33–36.

Fullea, J., Fernández, M. & Zeyen, H., 2008. FA2BOUG-A FORTRAN 90 code to compute Bouguer gravity anomalies from gridded free-air anomalies: application to the Atlantic-Mediterranean transition zone, *Comput. Geosci.,* **34**(12), 1665–1681.

Funck, T., Gohl, K., Damm, V. & Heyde, I., 2012. Tectonic evolution of southern Baffin Bay and Davis Strait: results from a seismic refraction transect between Canada and Greenland, *J. geophys. Res.,* **117**(B04107), doi:10.1029/2011JB009110.

Funck, T., Jackson, H., Louden, K. & Klingelhöfer, F., 2007. Seismic study of the transform-rifted margin in Davis Strait between Baffin Island (Canada) and Greenland: what happens when a plume meets a transform, *J. geophys. Res.,* **112**(B04402), doi:10.1029/2006JB004308.

Furlong, K. & Fountain, D., 1986. Continental crustal underplating: thermal considerations and seismic-petrologic consequences, *J. geophys. Res.,* **91**(B8), 8285–8294.

Gerlings, J., Funck, T., Jackson, H., Louden, K. & Klingelhöfer, F., 2009. Seismic evidence for plume-derived volcanism during formation of the continental margin in southern Davis Strait and northern Labrador Sea, *Geophys. J. Int.,* **176,** 980–994.

Gohl, K., Schreckenberger, B. & Funck, T., 2009. The expedition of the research vessel "Maria S. Merian" to the Davis Strait and Baffin Bay in 2008 (MSM09/3), in *Berichte zur Polar- und Meeresforschung (Reports on Polar and Marine Research),* Vol. 587, p. 104, eds Gohl, K., Schreckenberger, B. & Funck, T., Alfred Wegener Institute for Polar and Marine Research, Bremerhaven, ISSN: 1866-3192.

Gohl, K. & Smithson, S., 1993. Structure of Archean crust and passive margin of southwest Greenland from seismic wide-angle data, *J. geophys. Res.,* **98**(B4), 6623–6638.

Gohl, K. & Uenzelmann-Neben, G., 2001. The crustal role of the Agulhas Plateau, southwest Indian Ocean: evidence from seismic profiling, *Geophys. J. Int.,* **144**(3), 632–646.

Gradstein, F., Ogg, J. & Smith, A., 2004. *A Geological Time Scale 2004,* Cambridge University Press.

Gregersen, U. & Skaarup, N., 2007. A mid-Cretaceous prograding sedimentary complex in the Sisimiut Basin, offshore West Greenland - stratigraphy and hydrocarbon potential, *Mar. Pet. Geol.,* **24,** 15–28.

Holbrook, W. *et al.*, 2001. Mantle thermal structure and active upwelling during continental breakup in the North Atlantic, *Earth planet. Sci. Lett.,* **190,** 251–266.

Hopper, J., Dahl-Jensen, T., Holbrook, W., Larsen, H., Lizarralde, D., Korenaga, J., Kent, G. & Kelemen, P., 2003. Structure of the SE Greenland margin from seismic reflection and refraction data: implications for nascent spreading center subsidence and asymmetric crustal accretion during North Atlantic opening, *J. geophys. Res.,* **108**(B5), doi:10.1029/2002JB001996.

Keen, C. & Barrett, D., 1972. Seismic refraction studies in Baffin Bay: an example of a developing ocean basin, *Geophys. J. R. astr. Soc.,* **30,** 253–271.

Klose, G., Malterre, E., McMillan, N. & Zinkan, C., 1982. Petroleum exploration offshore southern Baffin Island, Northern Labrador Sea, Canada, in *Arctic Geology and Geophysics: Proceedings of the Third*

International Symposium on Arctic Geology, pp. 233–244, eds Embry, A. & Balkwill, H., Canadian Society of Petroleum Geologists, Calgary, Alberta.

Larsen, L., Rex, D., Watt, W. & Guise, P., 1999. ^{40}Ar-^{39}Ar dating of alkali basaltic dykes along the southwest coast of Greenland: Cretaceous and Tertiary igneous activity along the eastern margin of the Labrador Sea, *Geol. Greenland Surv. Bull.,* **184,** 19–29.

Lawver, L. & Müller, R., 1994. Iceland hotspot track, *Geology,* **22,** 311–314.

Mackenzie, G., Thybo, H. & Maguire, P., 2005. Crustal velocity structure across the Main Ethiopian Rift: results from two-dimensional wide-angle seismic modelling, *Geophys. J. Int.,* **162**(3), 994–1006.

Marillier, F. & Reid, I., 1990. Crustal underplating beneath the carboniferous Magdalen basin (Eastern Canada): evidence from seismic reflection and refraction, in *The Potential of Deep Seismic Profiling for Hydrocarbon Exploration,* pp. 209–218, eds Pinet, B. & Bois, C., Editions Technip, Paris.

Maus, S. *et al.*, 2009. EMAG2: A 2-arc min resolution Earth magnetic anomaly grid compiled from satellite, airborne, and marine magnetic measurements, *Geochem. Geophys. Geosyst.,* **10**(Q08005), doi:10.1029/2009GC002471.

McKenzie, D. & Bickle, J., 1988. The volume and composition of melt generated by extension of the lithosphere, *J. Petrol.,* **29**(3), 625–679.

Mjelde, R., Raum, T., Myhren, B., Shimamura, H., Murai, Y., Takanami, T., Karpuz, R. & Næss, U., 2005. Continent-ocean transition on the Vøring Plateau, NE Atlantic, derived from densely sampled ocean bottom seismometer data, *J. geophys. Res.,* **110**(B05101), doi:10.1029/2004JB003026.

Oakey, G., 2005. Cenozoic evolution and lithosphere dynamics of the Baffin Bay-Nares Strait region of Arctic Canada and Greenland, *PhD thesis,* Vrije Universiteit, Amsterdam.

Olesen, O. *et al.*, 2007. An improved tectonic model for the Eocene opening of the Norwegian-Greenland Sea: use of modern magnetic data, *Mar. Pet.Geol.,* **24,** 56–66.

Pedersen, A., Larsen, L., Pedersen, G. & Dueholm, K., 2006. Five slices through the Nuussuaq Basin, West Greenland, *Geol. Surv. Denmark Bull.,* **10,** 53–56.

Rice, P. & Shade, B., 1982. Reflection seismic interpretation and seafloor spreading history of Baffin Bay, in *Arctic Geology and Geophysics: Proceedings of the Third International Symposium on Arctic Geology,* pp. 245–265, eds Embry, A. & Balkwill, H., Canadian Society of Petroleum Geologists, Calgary, Alberta.

Roest, W. & Srivastava, S., 1989. Sea-floor spreading in the Labrador Sea: a new reconstruction, *Geology,* **17,** 1000–1003.

Rudnick, R. & Fountain, D., 1995. Nature and composition of the continental crust: a lower crustal perspective, *Rev. Geophys.,* **33**(3), 267–309.

Sandwell, D. & Smith, W., 2009. Global marine gravity from retracked Geosat and ERS-1 altimetry: ridge segmentation versus spreading rate, *J. geophys. Res.,* **114**(B01411), doi:10.1029/2008JB006008.

Skaarup, N., Jackson, H. & Oakey, G., 2006. Margin segmentation of Baffin Bay/Davis Strait, eastern Canada based on seismic reflection and potential field data, *Mar. Pet. Geol.,* **23,** 127–144.

Sleep, N., 1997. Lateral flow and ponding of starting plume material, *J. geophys. Res.,* **102**(B5), 10 001–10 012.

Smith, W. & Sandwell, D., 1997. Global seafloor topography from satellite altimetry and ship depth soundings, *Science,* **277,** 1957–1962.

Sørensen, A., 2006. Stratigraphy, structure and petroleum potential of the Lady Franklin and Maniitsoq Basins, offshore southern West Greenland, *Pet. Geosci.,* **12,** 221–234.

Srivastava, S., 1978. Evolution of the Labrador Sea and its bearing on the early evolution of the North Atlantic, *Geophys. J. R. astr. Soc.,* **52,** 313–357.

Srivastava, S., MacLean, B., Macnab, R. & Jackson, H., 1982. Davis Strait: structure and evolution as obtained from a systematic geophysical survey, in *Arctic Geology and Geophysics: Proceedings of the Third International Symposium on Arctic Geology,* pp. 267–278, eds Embry, A. & Balkwill, H., Canadian Society of Petroleum Geologists, Calgary, Alberta.

Storey, M., Duncan, R., Larsen, A. & Larsen, H., 1998. ^{40}Ar/^{39}Ar geochronoly of the West Greenland Tertiary volcanic province, *Earth planet. Sci. Lett.,* **160,** 569–586.

Suckro, S. *et al.*, 2012. The crustal structure of southern Baffin Bay: implications from a seismic refraction experiment, *Geophys. J. Int.,* **190**(1), 37–58.

Talwani, M. & Eldholm, O., 1977. Evolution of the Norwegian-Greenland Sea, *Geol. Soc. Am. Bull.,* **88,** 969–999.

Tessensohn, F. & Piepjohn, K., 2000. Eocene compressive deformation in Arctic Canada, North Greenland and Svalbard and its plate tectonic causes, *Polarforschung,* **68,** 121–124.

Verhoef, J., Roest, W., Macnab, R. & Arkani-Hamed, J., 1996. Magnetic anomalies of the Arctic and North Atlantic oceans and adjacent land areas, in *Open File Report 3125A,* Geological Survey of Canada, Calgary, Canada.

Voss, M. & Jokat, W., 2007. Continent-ocean transition and voluminous magmatic underplating derived from p-wave velocity modelling of the east Greenland continental margin, *Geophys. J. Int.,* **170**(2), 580–604.

White, R. & McKenzie, D., 1989. Magmatism at rift zones: the generation of volcanic continental margins and flood basalts, *J. geophys. Res.,* **94**(B6), 7685–7729.

White, R., McKenzie, D. & O'Nions, R.K., 1992. Oceanic crustal thickness from seismic measurements and rare Earth element inversion, *J. geophys. Res.,* **97**(B13), 19 683–19 715.

Zelt, C. & Smith, R., 1992. Seismic traveltime inversion for 2-D crustal velocity structure, *Geophys. J. Int.,* **108,** 16–34.

APPENDIX A: RAYTRACING IN THE *P*-WAVE VELOCITY MODEL FOR ALL OBS

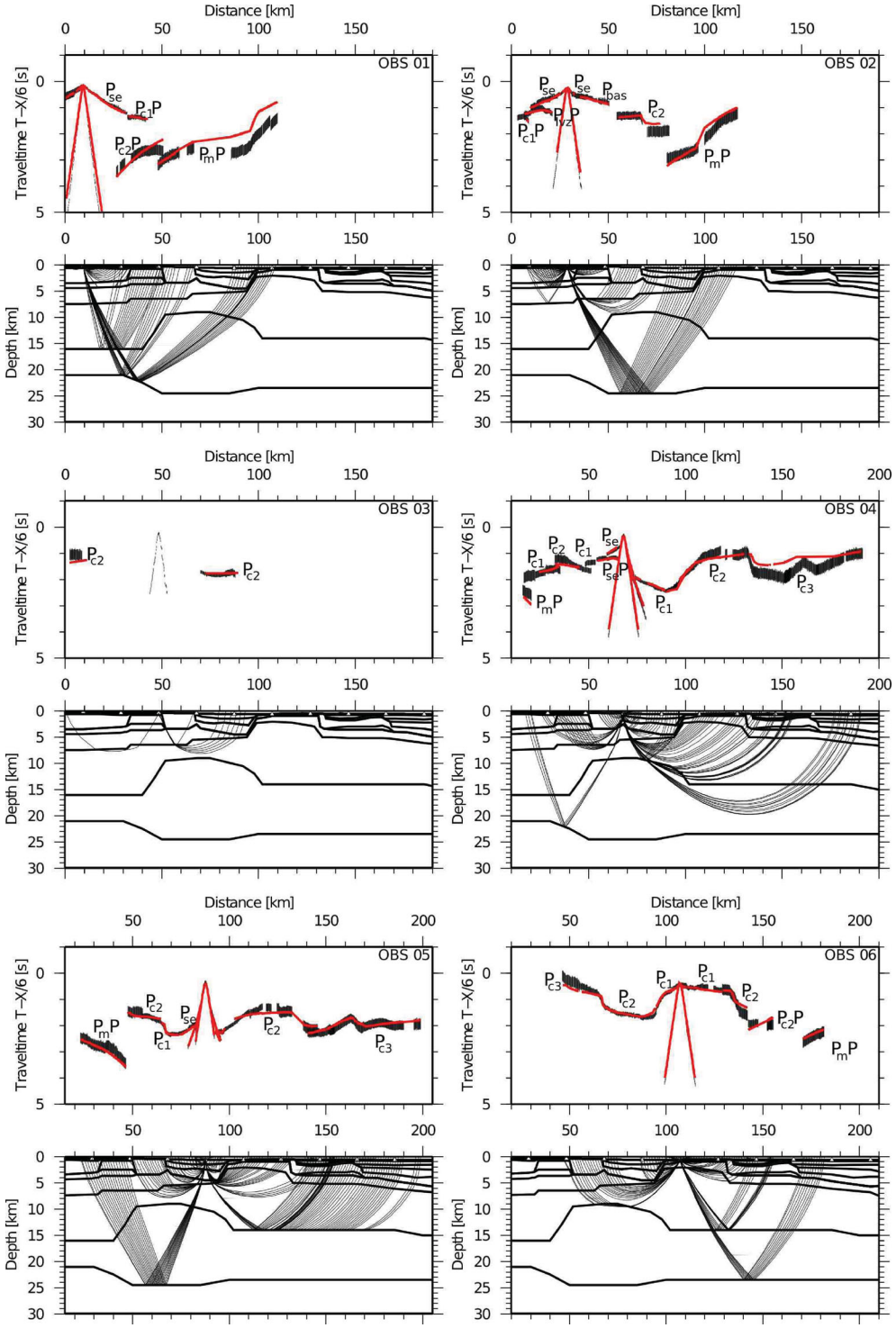

Figure A1. Raytracing in the *P*-wave velocity model for OBS 1–6. (Top panels) Picked phases in red with vertical bar length according to the assigned pick uncertainty; calculated traveltimes as thin black lines; phase names are annotated; a reduction velocity of 6 km s^{-1} is used. (Lower panels) Raypaths of the corresponding phases in the *P*-wave velocity model. For clarity, only every 10th ray is plotted.

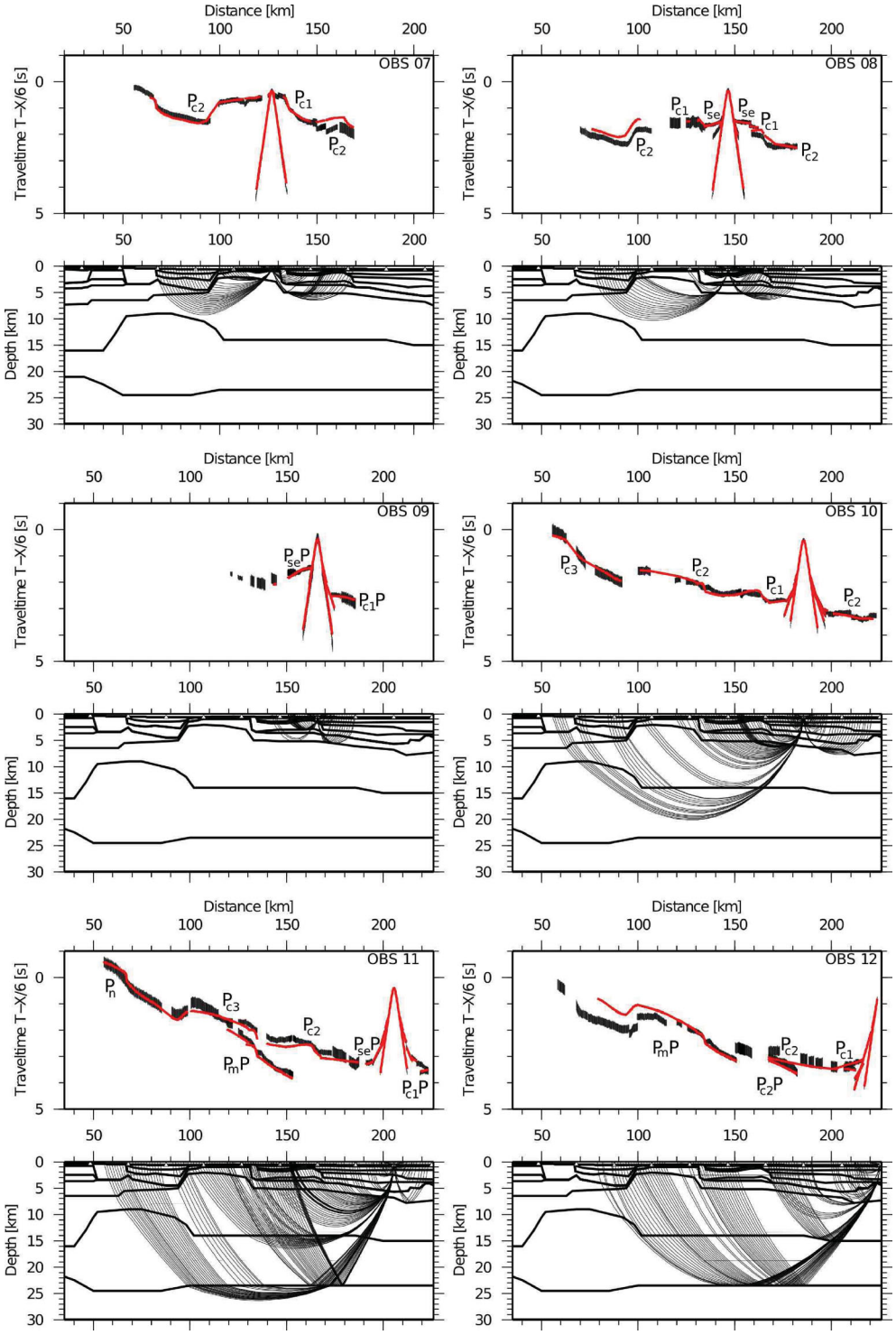

Figure A2. Raytracing in the *P*-wave velocity model for OBS 7–12. (Top panels) Picked phases in red with vertical bar length according to the assigned pick uncertainty; calculated traveltimes as thin black lines; phase names are annotated; a reduction velocity of 6 km s^{-1} is used. (Lower panels) Raypaths of the corresponding phases in the *P*-wave velocity model. For clarity, only every 10th ray is plotted.